

## Article

# Selective Neodymium Enrichment of Sulfides as a “Fingerprint” of Late Processes of Ore-Formation: Insight into Sm-Nd Isotopes for Sulfides from Magmatic Cu-Ni-PGE Complexes and Hydrothermal Pb-Zn, Au-Mo, and Gold Deposits

Pavel A. Serov 

Geological Institute of the Kola Science Centre, Russian Academy of Sciences, 184209 Apatity, Russia;  
serov@geoksc.apatity.ru

**Abstract:** The effect of enrichment with Nd in sulfides from magmatic Cu-Ni-PGE complexes and sulfide ores from hydrothermal Pb-Zn, Au-Mo, and gold deposits was found and characterized. This paper concerns the report and analysis of isotopic geochemical data on the sulfide ores from the large Paleoproterozoic mafic-ultramafic magmatic Cu-Ni-PGE complexes of Fennoscandia and the literature data on sulfide ores from the Qingchengzi Pb-Zn deposit (northeastern China), Tokuzbay gold deposit (southern Altai, northwestern China), and Dahu Au-Mo deposit (central China). The mineral/rock partition coefficients for Nd and Sm (the  $D_{Nd}/D_{Sm}$  ratio) are defined as a prospective tool for the reconstruction of the sulfide mineral formation and geochemical substantiation of possible sources of ore-forming fluids for deposits of various genetic types. The observed selective Nd accumulation indicates either hydrothermal or metamorphic (metasomatic) impact, which is associated with increased Nd mobility and its migration or diffusion. Due to this process, there is a relative Nd accumulation in comparison with Sm and a consequent increase in the  $D_{Nd}/D_{Sm}$  ratio. At the isotopic system level, this leads to a sufficient decrease in the Sm/Nd ratio for the secondary sulfides of such kind. The revealed effect may serve as an isotopic geochemical marker of recent processes. These processes are quite frequently associated with the most important ore formation stages, which bear the commercially valuable concentrations of ore components. Sulfides from magmatic Cu-Ni-PGE complexes are more characterized by the selective accumulation of Nd in the sequential sulfide mineral formation. For sulfides from hydrothermal deposits, the effect of Nd enrichment is more intense and closely related to ore-forming fluids, under the influence of which sulfide mineralization is formed in multiple stages. The study aims at expanding the knowledge about fractionation and the behavior of lanthanides in ore-forming processes and allows the development of additional criteria for the evaluation of the ore potential of deposits with different geneses, ages, and formation conditions.

**Keywords:** sulfides; REE distribution; silicate inclusions; Fennoscandian Shield; Cu-Ni-PGE ores; Pb-Zn deposit; Au-Mo deposit; gold deposit



**Citation:** Serov, P.A. Selective Neodymium Enrichment of Sulfides as a “Fingerprint” of Late Processes of Ore-Formation: Insight into Sm-Nd Isotopes for Sulfides from Magmatic Cu-Ni-PGE Complexes and Hydrothermal Pb-Zn, Au-Mo, and Gold Deposits. *Minerals* **2022**, *12*, 1634. <https://doi.org/10.3390/min12121634>

Academic Editors: Mauro César Geraldes and Guilherme Loriato Potratz

Received: 17 November 2022

Accepted: 17 December 2022

Published: 19 December 2022

**Publisher’s Note:** MDPI stays neutral with regard to jurisdictional claims in published maps and institutional affiliations.



**Copyright:** © 2022 by the author. Licensee MDPI, Basel, Switzerland. This article is an open access article distributed under the terms and conditions of the Creative Commons Attribution (CC BY) license (<https://creativecommons.org/licenses/by/4.0/>).

## 1. Introduction

During the last decades, the Sm-Nd system application has gone far beyond the classical techniques of dating the ancient mafic-ultramafic rocks and minerals composing those rocks (e.g., pyroxene, plagioclase, garnet, amphibole). At present, the use of the Sm-Nd system of sulfide minerals for dating the ore process and revealing the sources of ore matter of Cu-Ni-PGE, Au-Mo, Pb-Zn-Ag, and other deposits is becoming more and more popular. The obtained results hold out the prospect of the wider use of this method [1–8]. Numerous studies concerning the ore-magmatic system evolution generally assume the application of isotopic geochronological methods. The obtained results contribute much

to the study of ore-forming processes and ore component sources. They also allow the scientists to come right up to the creation of genetic models of the deposits.

Furthermore, the geochronological studies of Nd isotopes (alongside Sr and Pb isotopes) may be used in geochemical theory. Though the forms of REE occurrence in sulfides are to be debated [9–18], their isotopic geochemical markers are successfully used in the monitoring of the syngenetic and epigenetic conditions of deposit formation. Moreover, the markers often serve as a key to understanding the evolution of fluids that are responsible for sulfide mineralization [8,14]. However, the substantiation of REE isomorphism in a sulfide mineral structure nowadays is of hypothetical nature. It is partially proven for the hydrothermally generated sulfides only. In spite of this, different researchers quite confidently postulate the fact that the character of REE distribution in sulfide inherits its composition from ore-bearing fluid, which has influenced the formation of sulfide minerals [19,20].

Earlier, an important observation was made in the result of the analysis of entire Sm-Nd isotopic data available on sulfide minerals and their host rocks from the Paleoproterozoic Cu-Ni-PGE deposits of the Fennoscandian Shield. The isotopic geochemical markers were set for each particular deposit by way of defining the ratio of Nd and Sm concentrations in sulfides and parent rocks ( $D_{Nd}$  and  $D_{Sm}$  coefficients). The entire amount of data allowed the determination of the limits of these variations for different sulfide minerals, i.e., pyrite, pyrrhotine, chalcopyrite, pentlandite, and the sulfide mixed fractions. The obtained coefficients for sulfides from the different deposits showed a wide dispersion of values, but at the same time, the  $D_{Nd}/D_{Sm}$  ratio proved to be more stable and demonstrated fairly limited variations for the primary sulfide minerals, i.e., syngenetic ones or the sulfides of the early stages of ore genesis [1]. The analysis of obtained data revealed that, generally, the  $D_{Nd}/D_{Sm}$  ratio value increases sharply for the minerals of recent processes, which corresponds to the redeposition of ores, metamorphism, or hydrothermal impact. The observed effect of increasing the  $D_{Nd}/D_{Sm}$  ratio value is caused by a selective accumulation of Nd (relative to Sm) in sulfides and may be utilized as an indicator of a secondary process of sulfide formation at the recent stages of composition of the deposits and also as an indicator of the redeposition of sulfides, metasomatism, fluid impact, etc. [1]. Developing the idea, in our paper, we present and analyze isotopic geochemical data on the sulfide ores from the large Fennoscandian Paleoproterozoic mafic–ultramafic Cu-Ni-PGE complexes, i.e., ore deposits of Finland and the Russian Arctic Zone (Kola Peninsula and Karelia), and the literature data on the sulfide ores from the Qingchengzi Pb-Zn deposit (northeastern China), Tokuzbay gold deposit (south Altai, northwestern China), Dahu Au-Mo deposit, and Salla-Kuolajarvi albitites (Mo-bearing Ozernoe, Karelia). Thus, we were able to study not only magmatic Cu-Ni-PGE complexes but also deposits closely related to hydrothermal processes, i.e., clearly different in their genesis and formation conditions. This allowed us to obtain new data on REE fractionation during late hydrothermal processes in economically significant deposits and expand our understanding of the geochemistry of rare-earth elements in sulfide minerals.

## 2. Geological Settings

### 2.1. Magmatic Cu-Ni-PGE and Fe-Ti-V Complexes of the Fennoscandian Shield

In the northeastern part of the Fennoscandian Shield are large-scale mafic–ultramafic deposits of platinum-group elements (PGE), Cu-Ni-Co, and Fe-Ti-V. There are economically significant, especially the deposits containing critical raw materials, such as PGE, Ti, Co, and V (Figure 1). There are major Cu-Ni-Cr deposits in the Monchegorsk ore district [21–24] and Pechenga [25–28], Kolvitsa Fe-Ti-V deposit [29,30], PGE-bearing Fedorovo-Pansky complex [4,5,31–33], and Burakovsky intrusion [34], and Cu-Ni-PGE deposits in Finland, i.e., Kemi [24,35], Penikat [36], Portimo [37], Akanvaara, Koitelainen [38], Tornio [37], etc.

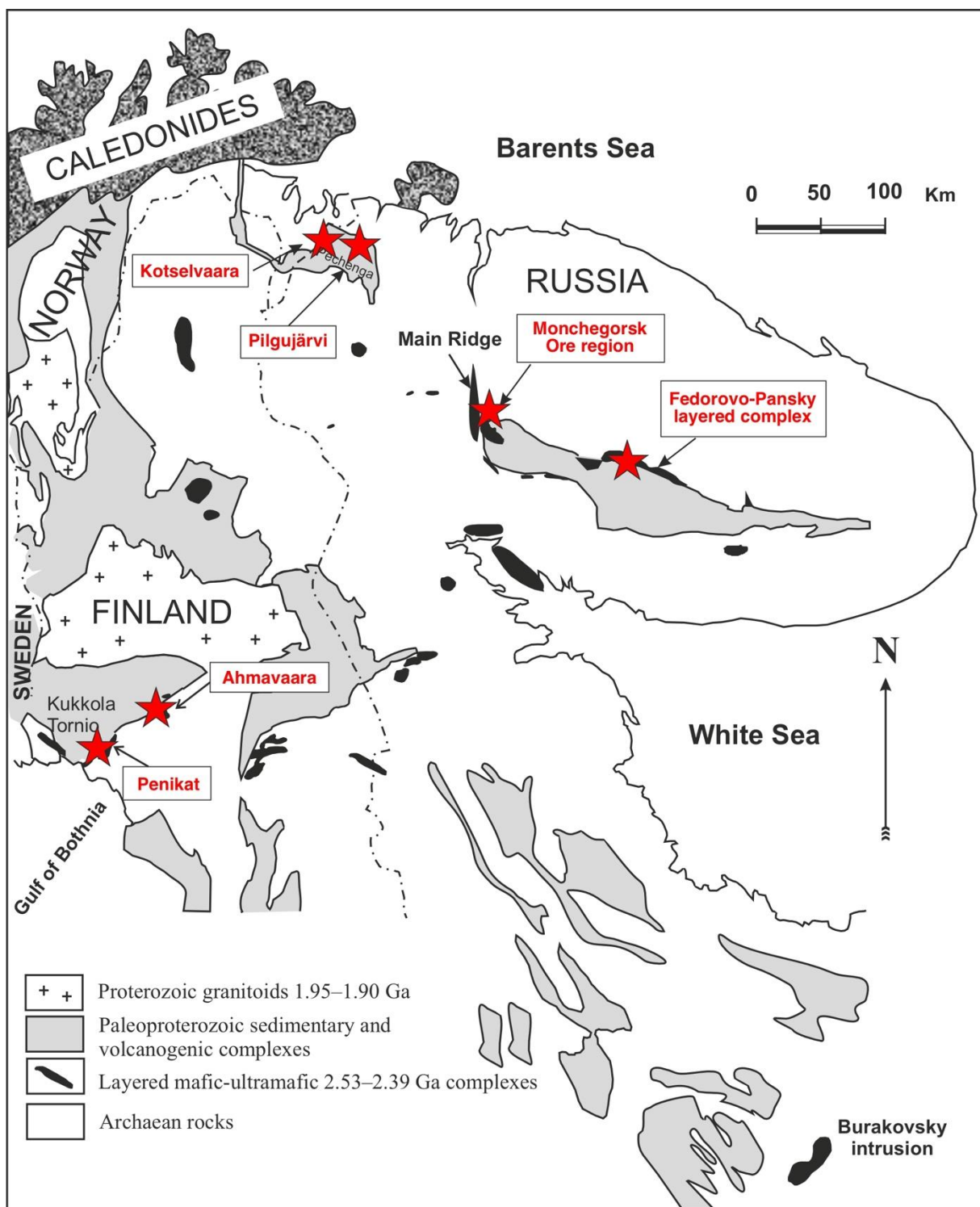


**Figure 1.** Generalized geological map of the northeastern part of the Fennoscandian Shield and the location of main Paleoproterozoic mafic–ultramafic Cu–Ni complexes (modified from [1]. Red asterisks indicate sampling locations).

The dated deposits were formed in two major episodes of 2.53–2.39 Ga and 2.0–1.8 Ga, corresponding to the early [1,5,24,25,33,39–51] and late [25–28,52,53] stages of rifting in the Fennoscandian Shield.

### 2.1.1. Pilgujärvi Cu-Ni Deposit

The Pilgujärvi Cu-Ni deposit occurs in the central part of the Pechenga ore field [28,53]. The deposit is associated with the peridotite lower parts of the differentiated intrusions. The ore formation at the age of 1.98 Ga and sulfide segregation are syngenetic in relation to the injection of intrusions, differentiation, and cooling of the nickel-bearing magma [26,28].

### 2.1.2. Kaula-Kotselvaara, Pechenga

The Kotselvaara massif is essentially an interstratal intrusive body in the tufogenic sedimentary rocks of the Pechenga western ore field [25,54]. The intrusion is vividly differentiated into three zones (from bottom to top): serpentinites (about 70% of volume), pyroxenites (5%–6%), and gabbro (24%–25%).

The majority of the sulfide copper–nickel mineralization is concentrated at the bottom part of the massif, mainly in peridotites and pyroxenites. Small amounts of Ni and Cu are known to occur in gabbro. The copper–nickel ores can be divided into four main types according to their composition and structure [55]. These are (1) disseminated ores in serpentinites (modified peridotites); (2) breccia ores; (3) massive sulfide ores; and (4) vein-disseminated ores in schists.

Over the course of metamorphism, the most intense processes of the desulfidation and oxidation of primary sulfides take place in massive and breccia ores, after which magnetite, violarite, and siderite accompanied by chlorite, talc, and dolomite metasomatically occur.

### 2.1.3. Ahmavaara Deposit, Portimo Complex (Finland)

The Portimo complex includes the Narkaus and Sukhanko-Konttijärvi intrusions, with a crystallization age of 2.44 Ga, which are presumably related to a coeval swarm of dikes known as the Portimo dikes [37]. It is assumed that this complex was formed due to two different magmas, and the early magma was richer in MgO, Cr, and LPEE than the later magma. Both magmas contain low contents of TiO<sub>2</sub> and belong to the boninite series [56].

### 2.1.4. Monchegorsk Ore Field

The Monchegorsk ore field includes rocks of the ore-bearing Monchepluton, gabbro–anorthosite massifs of the Monchetundra and Chunatundra, Ostrovskoy, and Yarva-Varaka intrusions, and a dike swarm cutting through the Monchepluton [23,42,57]. The complex formed in an interval of 2.51–2.46 Ga [33,42,58].

Monchepluton has an arcuate shape and consists of two branches (or chambers). The northwestern branch is represented by the Nittis–Kumuzhya–Travyanaya (or NKT) massifs, and the branch nearby from east to west is composed of the Sopcha–Nyud–Poaz and Vurechuayvench massifs. The complex is composed of dunites, harzburgites, orthopyroxenites (NKT), orthopyroxenites (Sopcha), norites (Nyud), and gabbro-norites (Poaz and Vurechuayvench), which form a single syngenetic rock sequence. It is clearly differentiated both vertically and horizontally, which is generally expressed in the reduced basicity of the rocks from the bottom up and from west to east [23,41,42].

### 2.1.5. Fedorovo-Pansky 2.5 Ga Layered Complex

The Fedorovo-Pansky layered complex occurs in the central part of the Kola Peninsula at the boundary of the Early Proterozoic volcanic-sedimentary rift series and Archean basement gneisses. The Fedorovo-Pansky complex is mainly represented by gabbro-norites with different contents of dark-colored minerals and various structural features. From bottom to top, the layered sequence looks like this [5,31,33]: amphibole schists, which belong to hardened marginal rocks; a taxite zone (30–300 m) containing ore-bearing gabbro-norites (2485 Ma), and xenoliths of pyroxenites and norites (2526–2516 Ma). Syngenetic ores are represented by copper and nickel sulfides, as well as platinum and palladium sulfides, bismuth tellurides and arsenides, and a Noritic zone (50–200 m) with interbeds of harzburgites and pyroxenites.

### 2.2. Tokuzbay Gold Deposit (South Altai, Northwest China)

The geological structure of the Tokuzbay gold deposit is rather simple. It is associated with permeable shear zones. The ore zones comprise metasandstones, phyllites, and crystalline limestones of the Altai suite. The ore bodies are limited by the faults of northwestern trending [6]. Magmatic fields are widely distributed in the area, including plagioclase granites and dikes of diorite and granite–porphyry that cut through the granites. The plagioclase granites, granite–porphyries, and diorite dikes were formed at  $406.3 \pm 2.1$  Ma [59],  $384.1 \pm 1.5$  Ma [60], and  $375.5 \pm 4.8$  [61] Ma, respectively.

Four stages of mineral formation are distinguished within the deposit, the third stage being the main ore-forming one. The gold-bearing quartz veins were intruded in the diorite dikes as well as in metasediments, thus forming the disseminated ores [6]. The age of sulfide mineralization associated with gold mineralization formation is ca. 292 Ma ( $^{39}\text{Ar}/^{40}\text{Ar}$  method) [62].

### 2.3. Qingchengzi Pb-Zn (Northeastern China)

The Qingchengzi ore field is located on the Liaodong Peninsula, in the northeastern part of the North China Craton. It comprises the Archean and Paleoproterozoic basement rocks, overlaid by the Mesoproterozoic–Cenozoic sedimentary cover [63].

Volcanogenic sedimentary rocks of the Liaohe Group (2.2–2.0 Ga) rest with unconformity on the Late Archean rocks. They host giant non-ferrous and precious metal deposits, including world-class magnesite, borate, and Pb-Zn-Au-Ag deposits [18,64]. The Liaohe group is divided into five formations, i.e., Langzishan, Lieryu, Gaojiayu, Dashiqiao, and Gaixian [65]. The Dashiqiao Formation is the main ore-bearing bed of the Pb-Zn ore bodies, whereas the Ag-Au ore bodies may be found mostly in the Gaixian Formation [66].

Four stages of mineralization are distinguished, i.e., (1) dolomite–quartz–pyrite; (2) pyrite–arsenopyrite–sphalerite–galena–chalcopyrite; (3) sulfides–quartz–carbonate; and (4) carbonate with minor sulfides. Pyrite occurs at all stages but decreases in amount from the early to late stages [67]. The Pb-Zn mineralization age is consistent with the age of the intrusion of the Late Jurassic granites in this region ( $151.8 \pm 5.2$  Ma) [18].

### 2.4. Dahu Au-Mo Deposit

The Dahu Au-Mo deposit is a structurally limited deposit system situated in the northern part of the Xiaoqinling terrane (the second largest gold province in China), Qinling orogen.

The Dahu Au-Mo deposit is situated on the northern margin of the Xiaoqinling terrane and comprises biotite-plagioclase and migmatite gneisses of the Taihua Supergroup [7]. Gold and molybdenum mineralization is associated with a series of quartz veins limited by the faults of northeastern and northwestern trending.

A hydrothermal process that formed the ore system of the Dahu Au-Mo deposit may be divided into four stages, i.e., (1) brecciated coarse-grained molybdenite–pyrite veins; (2) fine-grained quartz–molybdenite–pyrite–gold veinlets and phenocrysts; (3) quartz–polymetallic sulfide–gold veins containing pyrite, chalcopyrite, galena, sphalerite, and other minerals; and (4) quartz–carbonate veins, sometimes containing pyrite. The second and third stages are called the “main mineralization stage” [68]. The Dahu Au-Mo deposit was formed in the Late Triassic, as the U-Th-Pb dating of hydrothermal monazite syngenetic with the early stage molybdenite yielded an age of  $216 \pm 5$  Ma [69]. The monazite also indicated a rejuvenated U-Th-Pb age close to 125 Ma, which suggests the idea that the Dahu mineral system was transformed as the result of a recent tectonic-thermal event, which in its turn led to the formation of large-scale gold mineralization in the Xiaoqinling terrane [69].

## 3. Samples and Methods

Sulfides from Paleoproterozoic rocks (2.53–1.98 Ga) of magmatic Cu-Ni-PGE deposits of the Fennoscandian Shield were studied by mass-spectrometric technique (Finnigan MAT-262, Waltham, MA, USA) and ICP-MS to define REE in samples.

Data for the Tokuzbay gold deposit (Southern Altai, North-Western China), Dahu Au-Mo deposit, and Salla-Kuolajarvi albitites (Ozernoe, Karelia) were taken from [6,7,18,70].

### 3.1. Sm-Nd Analytical Methods

The isotope research was carried out in the Collective Use Centre of the Kola Science Centre RAS (Apatity, Russia). In order to define concentrations of Sm and Nd, the sample was mixed with a compound tracer  $^{149}\text{Sm}/^{150}\text{Nd}$  prior to dissolution. It was then diluted with a mixture of HF + HNO<sub>3</sub> (or +HClO<sub>4</sub>) in Teflon sample bottles at a temperature of 100 °C until complete dissolution. Further extraction of Sm and Nd was carried out using standard procedures with two-stage ion exchange and extraction chromatographic separation using ion-exchange tar “Dowex” 50 × 8 in chromatographic columns employing 2.3 N and 4.5 N HCl as an eluent. The separated Sm and Nd fractions were transferred into a nitrate form, whereupon the samples (preparations) were ready for mass-spectrometric analysis.

The isotope Nd composition and Sm and Nd contents were measured by a 7-channel solid-phase mass-spectrometer, Finnigan-MAT 262 (Waltham, MA, USA), equipped with a Retarding Potential Quadrupole (RPQ) in a static double-band mode, using Ta + Re filaments. A mean value of  $^{143}\text{Nd}/^{144}\text{Nd}$  ratio in a JNdi-1 standard was  $0.512081 \pm 13$  (N = 11) in the test period. An error in  $^{147}\text{Sm}/^{144}\text{Nd}$  in ratios was 0.3% (2σ), which is the mean value of 7 measurements in a BCR-2 standard [71]. An error in the estimation of isotope Nd composition in an individual analysis was up to 0.01% for minerals with low Sm and Nd contents. The blank intralaboratory contamination was 0.3 ng in Nd and 0.06 ng in Sm. The accuracy of the estimation of Sm and Nd contents was ±0.5%. Isotope ratios were normalized per  $^{146}\text{Nd}/^{144}\text{Nd} = 0.7219$ , and then recalculated for  $^{143}\text{Nd}/^{144}\text{Nd}$  in JNdi-1 = 0.512115 [72]. The parameters of isochrons were estimated using the ISOPLOT program complex [73]. Values of εNd(T) and T(DM) model ages were estimated using present-day values of CHUR as described in [74] ( $^{143}\text{Nd}/^{144}\text{Nd} = 0.512630$ ,  $^{147}\text{Sm}/^{144}\text{Nd} = 0.1960$ ) and DM as described in [75] ( $^{143}\text{Nd}/^{144}\text{Nd} = 0.513151$ ,  $^{147}\text{Sm}/^{144}\text{Nd} = 0.2136$ ).

### 3.2. ICP-MS

To define REE in samples with no preliminary separation and concentration, reference values of REE concentrations in the GSO 2463 standard (apatite), sulfide from the Talnakh deposit, and international standard samples from the Centre of Petrographic and Geochemical Research (Nancy, France) were reproduced using the ELAN 9000 DRC-e (Perkin Elmer, Waltham, MA, USA) quadrupole mass-spectrometer at the Tananaev Institute of Chemistry KSC RAS (Apatity, Russia). The samples were separated under the conditions provided in [76].

The analysis was based on the following parameters: plasma power of 1300–1350 W; sprayer gas flow (high-clean Ar) within 0.75–1.0 L/min<sup>-1</sup>; ion lens voltage < 11 V; and level of doubly charged and oxide ions < 2.5%. A geological sample weighing up to 100 mg in the polystyrene hermetically sealed test tube mixed with distilled acids (HNO<sub>3</sub>, HF, HCl 5 mL each) was exposed to a water bath at a temperature of 50–60 °C until fully dissolved. No HCl was added in the course of the opening of sulfide minerals. When opening the sample, we registered an increased pressure of acid and nitrogen oxide vapor that suppressed the volatility of the components in the sample. The chilled sample was mixed with 0.1 mL H<sub>2</sub>O<sub>2</sub>, and the dissolved sample was diluted with 2% HNO<sub>3</sub>. The level of total REE content in the blank sample was <0.5 ppb. This blank sample qualifies the level of analytical accuracy and the limit of element detection. Since the samples have yielded high concentrations of those elements that may cause matrix effects and ion interference, the calibration curves were plotted with an interfering agent added to the blank calibration solution. The multicomponent standard solutions by Perkin Elmer (“Multi-element ICP-MS Calibration Std”) were used. The sample itself was selected as an interfering agent. The amount of the interfering agent was chosen so that the macrocomponent concentration after mixing exceeded the REE concentration in the calibration solution by a factor of 100. The

approximation linearity of the REE correction curves is  $\geq 99.99\%$ . Spectral superimposition was recognized by ELAN 9000 DRC-e MS software (Perkin Elmer, Waltham, MA, USA) and adjusted by the introduction of correction equations into the analytic program defined with reference to the natural abundance of REE isotopes. The blank sample solution free of the interfering agent was used to analyze the solution of the opened sample.

### 3.3. Coefficients Sulfide/Whole Rock

The coefficients of sulfide/whole rock were calculated according to the equations:

$$D_{Nd} = [Nd]_{Sulf} / [Nd]_{WR}$$

$$D_{Sm} = [Sm]_{Sulf} / [Sm]_{WR}$$

where  $D_{Nd}$  and  $D_{Sm}$  are the sulfide/rock partition coefficients for Nd and Sm;  $[Nd]_{Sulf}$  and  $[Sm]_{Sulf}$ —concentration of Nd and Sm in sulfide; and  $[Nd]_{WR}$  and  $[Sm]_{WR}$ —concentration of Nd and Sm in the whole rock (WR).

## 4. Results and Discussion

The presented results are based on a regularly updated analytical Sm-Nd database. It concerns sulfides from the large Precambrian magmatic Cu-Ni-Cr-PGE deposits and ore occurrences of the Fennoscandian Shield and the western part of the Russian Arctic (Table 1). Some parts of the database were published in [1,33,70,77,78]. The literature data were used to analyze and establish the rules of REE behavior in sulfides from the hydrothermal Pb-Zn, Au-Mo, and orogenic gold deposits (references are given in the table against the names of the deposits). There are Sm-Nd data on each studied deposit for the sulfides (often represented by the sulfides from several stages) as well as for the rocks encompassing these sulfides (Table 1). This allowed us to calculate sulfide/rock coefficients for neodymium ( $D_{Nd}$ ) and samarium ( $D_{Sm}$ ) and define their ratio ( $D_{Nd}/D_{Sm}$  “marker”).

**Table 1.** Neodymium and samarium concentrations in sulfide minerals from the magmatic and hydrothermal complexes and the respective  $D_{Nd}/D_{Sm}$  ratio values.

Sample	Rock and Geological Setting	Concentrations in Sulfide, ppm		Concentrations in Whole Rock, ppm		$D_{Nd}/D_{Sm}$
		Sm	Nd	Sm	Nd	
		Monchegorsk area (Kola Peninsula, Russia)				
1	B58/111 Mix	0.030	0.120	0.970	4.62	0.83
2	B58/111 Pn	0.109	0.350	0.970	4.62	0.67
3	B70/111 Mix	0.034	0.188	0.041	0.131	1.73
4	MT-3 Mix	0.020	0.090	0.245	1.055	1.05
5	P-1/109 Mix	0.032	0.123	0.678	2.09	1.23
6	P-1/109 Po	0.018	0.095	0.678	2.09	1.73
		Fedorovo-Pansky complex (Kola Peninsula, Russia)				
7	FPM-1 Ccp	0.049	0.248	0.563	3.12	0.91
8	FPM-1 Po	0.028	0.176	0.563	3.12	1.14
9	FPM-1 Po-2	0.073	0.294	1.132	6.01	0.75
10	FPM-1 Ccp + Pn	0.022	0.122	1.044	4.99	1.14
11	FPM-1 Mix	0.424	1.663	0.563	3.120	0.71
12	MP-1 Po	0.029	0.151	1.044	4.99	1.11
13	BGF-616 Py + Pn	0.153	0.912	1.313	5.77	1.36
14	BGF-616 Py	0.082	0.452	1.313	5.77	1.26
15	BGF-616 Py	0.157	0.934	2.49	8.41	1.76
16	BGF-616 Ccp	0.104	0.597	1.313	5.77	1.30
		Pechenga (Kola Peninsula, Russia)				
17	Pilg-4/3 Pn	0.040	0.210	0.26	1.700	0.80
18	Pilg -4/3 Po	0.180	2.180	0.260	1.700	1.85
19	Pilg-4/3 Mix	0.070	1.050	0.260	1.700	2.29

Table 1. Cont.

Sample	Rock and Geological Setting	Concentrations in Sulfide, ppm		Concentrations in Whole Rock, ppm		D <sub>Nd</sub> /D <sub>Sm</sub>		
		Sm	Nd	Sm	Nd			
20	Pilg-4/3 Ccp	Massive ore (Pilgujärvi)		0.040	0.230	0.260	1.700	0.88
21	KT-10 Mix	Antigorite with sulfides (Kotselvaara)		0.291	1.221	0.260	1.700	0.64
22	KT-6 Mix	Sulfides from talc vein (Kotselvaara)		0.055	0.167	0.260	1.700	0.46
23	KT-8 Mix	Sulfides from a carbonate vein (Kotselvaara)		0.046	0.278	0.260	1.700	0.92
24	KT-9 Mix	Quartz-sulfide vein (Kotselvaara)		0.135	0.701	0.260	1.700	0.79
Finnish Group Intrusions, Finland								
25	F-6 Py	Gabbonorite (Penikat)		0.417	1.706	0.850	4.41	0.79
26	F-4 Mix	Gabbonorite (Penikat)		0.114	0.709	2.00	10.07	1.23
27	F-4 Py	Gabbonorite (Penikat)		0.117	0.767	2.00	10.07	1.31
28	F-4 Ccp	Gabbonorite (Penikat)		0.109	0.647	2.10	10.07	1.19
29	F-4 Po	Gabbonorite (Penikat)		0.301	2.020	2.00	10.07	1.32
30	F-8 Ccp	Gabbonorite (Penikat)		0.005	0.019	0.710	2.87	0.86
31	F-8 Pn	Gabbonorite (Penikat)		0.005	0.017	0.710	2.87	0.71
32	F-8 Pn	Gabbonorite (Penikat)		0.008	0.044	1.044	4.99	1.00
33	F-8 Mix	Gabbonorite (Penikat)		0.008	0.038	0.710	2.87	1.18
34	F-28 Ccp	Massive ores (Ahmavaara)		0.761	5.140	1.132	6.01	1.27
35	F-28 Pn	Massive ores (Ahmavaara)		0.151	0.842	1.132	6.01	1.05
36	F-28 Po	Massive ores (Ahmavaara)		0.073	0.394	1.132	6.01	1.02
Qingchengzi Pb-Zn deposits, northeastern China (data from [18])								
37	Py	Pb-Zn ores (Qingchengzi)		0.05	0.65	16.71	117.3	1.85
38	Py	Pb-Zn ores (Qingchengzi)		0.02	0.11	16.71	117.3	0.76
39	Py	Pb-Zn ores (Qingchengzi)		0.04	0.17	16.71	117.3	0.62
40	Py	Pb-Zn ores (Qingchengzi)		0.02	0.10	16.71	117.3	0.86
41	Py	Pb-Zn ores (Qingchengzi)		0.00	0.02	16.71	117.3	0.71
42	Py	Pb-Zn ores (Qingchengzi)		0.17	1.34	16.71	117.3	1.11
43	Py	Pb-Zn ores (Qingchengzi)		0.16	0.99	16.71	117.3	0.88
44	Py	Pb-Zn ores (Qingchengzi)		0.08	0.48	16.71	117.3	0.85
45	Py	Pb-Zn ores (Qingchengzi)		0.07	0.50	16.71	117.3	0.99
46	Py	Pb-Zn ores (Qingchengzi)		0.10	0.50	16.71	117.3	0.75
Tokuzbay gold deposit (south Altai, northwest China) (data from [6])								
47	26-1-3 Py	Disseminated ores (Stage-1)		0.36	1.41	2.73	13.1	0.82
48	S3 Py	Quartz-pyrite vein (Stage-2)		0.1	0.46	2.73	13.1	0.96
49	S1 Py	Quartz-pyrite vein (Stage-2)		0.07	0.39	2.73	13.1	1.16
50	TK-Py Py	Quartz-pyrite vein (Stage-2)		0.08	0.38	2.73	13.1	0.99
51	5-3-83-4 Py	Quartz-pyrite vein (Stage-2)		0.1	0.64	2.73	13.1	1.33
52	33-6-Py	Quartz-polymetallic sulfides vein (Stage-3)		0.09	0.60	2.73	13.1	1.39
53	33-6-Ccp	Quartz-polymetallic sulfides vein (Stage-3)		0.04	0.24	2.73	13.1	1.25
54	I-py	Quartz-polymetallic sulfides vein (Stage-3)		0.03	0.15	2.73	13.1	1.04
55	33-3 py	Quartz-polymetallic sulfides vein (Stage-3)		0.22	1.15	2.73	13.1	1.09
56	33-3-ccp	Quartz-polymetallic sulfides vein (Stage-3)		0.46	2.45	2.73	13.1	1.11
57	26-1-10 Py1	Disseminated ores (Stage-1)		0.59	2.57	3.14	10.18	1.34
58	26-1-a Py1	Disseminated ores (Stage-1)		0.75	2.71	3.14	10.18	1.11
59	26-1-1 Py1	Disseminated ores (Stage-1)		0.44	2.42	3.14	10.18	1.70
Redeposited, metamorphic, and hydrothermally altered ores								
60	KT-2 Mix	Disseminated ore (Kotselvaara)		0.100	2.546	0.260	1.700	3.89
61	KT-4 Mix	Massive ores (Kotselvaara)		0.013	0.322	0.260	1.700	3.79
62	F-27 Pn	Redeposited ores (Ahmavaara)		0.192	4.990	2.49	8.41	7.70
63	F-27 Ccp	Redeposited ores (Ahmavaara)		0.183	3.040	2.49	8.41	4.95
64	F-27 Po	Redeposited ores (Ahmavaara)		0.263	1.975	2.49	8.41	2.22
65	Ccp	Albitites Salla-Kuolajarvi (Karelia) [70]		0.762	10.52	2.66	6.01	6.11
66	TK-P1 Py3	Quartz-polymetallic sulfides vein (Stage-3) Tokuzbay gold deposit [6]		0.03	0.70	3.14	10.18	7.20
67	6-x-2 Py3	Quartz-polymetallic sulfides vein (Stage-3) Tokuzbay gold deposit [6]		0.04	0.25	3.14	10.18	1.93
68	B66/111 Py	Ore-bearing norites Nyud-II		0.029	0.168	1.322	3.46	2.21
69	B66/111 Ccp	Ore-bearing norites Nyud-II		0.082	0.556	1.322	3.46	2.59

Table 1. Cont.

Sample	Rock and Geological Setting	Concentrations in Sulfide, ppm		Concentrations in Whole Rock, ppm		$D_{Nd}/D_{Sm}$	
		Sm	Nd	Sm	Nd		
		Dahu Au-Mo deposit (data from [7])					
70	7-002-2 Py	Dahu Au-Mo deposit	0.06	0.62	4.90	16.98	2.98
71	7-005-3 Py	Dahu Au-Mo deposit	0.01	0.06	4.90	16.98	1.73
72	DH-3 Py	Dahu Au-Mo deposit	0.43	4.42	4.90	16.98	2.97
73	DH07-1 Py	Dahu Au-Mo deposit	0.13	1.16	4.90	16.98	2.58
74	DH07 Py	Dahu Au-Mo deposit	0.09	0.37	4.90	16.98	1.19
75	7-005-1 Py	Dahu Au-Mo deposit	0.01	0.12	4.90	16.98	3.47
76	7-002-1 Py	Dahu Au-Mo deposit	0.02	0.12	4.90	16.98	1.73
77	35-010-1 Py	Dahu Au-Mo deposit	0.08	0.62	4.90	16.98	2.24
78	DH-4 Gal	Dahu Au-Mo deposit	0.03	0.11	4.90	16.98	1.06
79	DH08-20 Gal	Dahu Au-Mo deposit	0.37	3.06	4.90	16.98	2.39
80	35-010-2 Gal	Dahu Au-Mo deposit	0.17	1.21	4.90	16.98	2.06

The mean concentrations of neodymium and samarium in host rocks calculated on the ground of [6,7,18] were applied in the calculation of the  $D_{Nd}/D_{Sm}$  ratio for the sulfides from the Qingchengzi Pb-Zn deposit, Tokuzbay gold deposit, and Au-Mo deposit.

The neodymium concentrations in the studied examples of sulfide minerals are defined within the 0.017–10.52 ppm range and samarium concentrations are defined within the 0.005–0.762 ppm range. Most of the studied sulfide minerals contain small amounts of ppm of Nd and Sm (Table 1).

#### 4.1. Forms of REE Occurrence in Sulfides

As a rule, the sulfides are REE-depleted because of the large difference in ionic radii between  $REE^{3+}$  (0.98–1.16 Å) and main cations, which impedes the replacement [79,80] of main cations by REE in the crystal lattice of a sulfide. On the other hand, it is defined that the mineral inclusions may control low-level REE concentrations in sulfide [1,81]. It is important to note that the sulfides forming in REE-rich environments may couple the first ppm of REE in their structure because of the lattice defects or adsorption [82,83].

Different scientists have proposed several hypotheses of REE occurrence in sulfides at various times:

- The isomorphic replacement of main cations in a lattice [9];
- Silicate micro-inclusions within the sulfide with a certain REE composition [10];
- REE occurrence in defects of the crystal lattice of a sulfide mineral [11,83];
- The sorption of light REE on the surface of sulfide minerals [12,82];
- The bulk composition of REE in a sulfide as a sum of the contributions of silicate and fluid inclusions and REE isomorphic admixture, as well [84,85].
- Fluid inclusions with inherited REE composition from an ore-bearing melt [8,13–19,86]. Many hydrothermal ore deposits are known to be formed by the interaction of ore fluids with the host rocks. Thus, the isotopic composition of ores depends on the isotopic composition of the host rocks and ore-forming fluids [7,87,88]. Notably, despite the publications where the REE occurrence in the form of fluid inclusions in hydrothermally generated sulfides is postulated, there are no pictures of these inclusions. This is probably caused by the difficulties of the optical detection of such inclusions due to the non-transparency of a sulfide mineral and the incapability of opening the sulfide without breaking a fluid inclusion capsule. Having taken this reason into consideration, we suggested that heterophase inclusions in the form of sub-micron bubbles of fluids or melt may be a possible source of REE in sulfides [1]. However, the results of the computer micro-tomography of disseminated ore sulfides from the Pilgūjärvi Cu-Ni deposit (Pechenga, Kola Peninsula) and ore gabbro-norites from the platinum-bearing Fedorovo-Pansky complex (Kola Peninsula) did not sup-

port this hypothesis, as the studied sulfide minerals showed their homogeneity to the scale of one micron [89]. The absence of silicate micro-inclusions of a size bigger than one micron in the studied sulfides allows us to suggest the isomorphic form of REE occurrence in sulfides. On the other hand, there is a hypothesis that the composition of REE silicate micro-inclusions is a part of a general balance of REE fluid from which the sulfide had crystallized. So, the bulk composition of REE in a mineral may be treated as a composition of an ore-forming fluid [10,84,85]. Otherwise, the neodymium isotopic anomalies in sulfides may also be the result of segregation in lattice defects and similar defects may serve as channels for a swift diffusion of elements [90].

#### 4.2. REE Distribution in Sulfides

Our earlier studies of REE distribution in the sulfides of the Cu-Ni ores from the northeastern Baltic Shield deposits (the Pilgijärvi deposit, Pechenga, and the Penikat intrusion, Finland) showed (Figure 2) that features of REE distribution in sulfides repeat the REE distribution in rock [1,76,91]. Similar patterns of REE distribution in sulfides are also noticed in many hydrothermal deposits, where the role of fluids and hydrothermal processes in ore genesis is crucial [7,18–20]. A similar pattern may be observed for the sulfides from black and white smokers, as it was previously shown that the REE structures in these sulfides bear a resemblance to the REE structures of the hydrothermal fluids [92,93]. As for the Rainbow hydrothermal field (the Mid-Atlantic Ridge), it was shown that the REE sulfide composition clearly depicts the REE structure with a sufficient enrichment of light REE [93]. The total REE composition in a sulfide can be taken as a reflection of the ore-forming fluid composition [10,84]. The distribution of REE in sulfide is part of the overall balance of REE in the ore-forming system. In the vast majority of cases, the inheritance pattern of REE distribution in the whole-rock and sulfide minerals is observed. Moreover, this effect is observed both in igneous and hydrothermal ore systems.

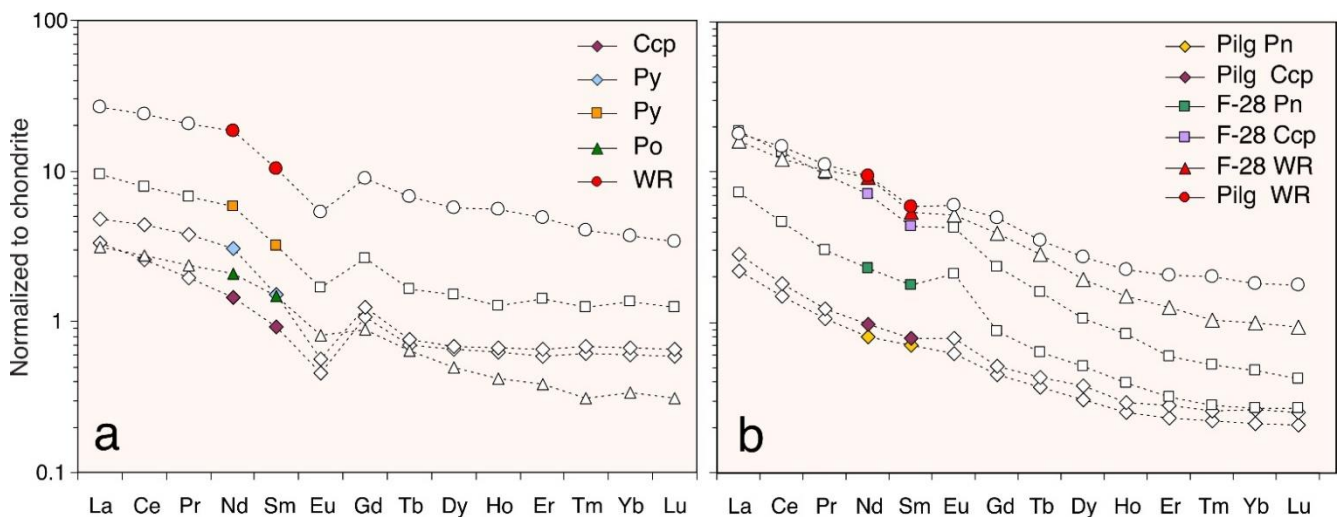


**Figure 2.** REE distribution in rock (WR) and sulfide minerals from magmatic Cu-Ni-PGE complexes of the Fennoscandian Shield: (a) Penikat intrusion, Finland; (b) Pilgijärvi Cu-Ni deposit (Pilg) and Ahmavaara intrusion (F-28). Pn—pentlandite; Ccp—chalcopyrite; Pn—pentlandite; Po—pyrrhotite; WR—whole rock.

#### 4.3. Selective Enrichment of Nd in Sulfides

Apart from the geochronological age determinations, an important observation connecting Nd and Sm concentrations in sulfides and rock was made as the result of the analysis of the entire Sm-Nd isotopic data available on sulfide minerals and their host rocks. Having defined the ratio of Nd and Sm concentrations in sulfides and rock ( $D_{Nd}$  and  $D_{Sm}$  coefficients), we managed to set up isotopic geochemical markers for each particular deposit, and the entire body of data allowed us to determine the limits of these variations

for different sulfide minerals, i.e., pyrite, pyrrhotine, chalcopyrite, pentlandite, and the sulfide mixed fractions [1]. The coefficients obtained for sulfides from the different deposits showed a wide dispersion of values (Figure 3), but at the same time, the  $D_{Nd}/D_{Sm}$  ratio proves to be more stable and varies within quite narrow limits for primary sulfide minerals, syngenetic, or sulfides of the early stages of mineral formation [1]. The  $D_{Nd}/D_{Sm}$  ratios were calculated on the basis of the entire body of analytical and literature data (80 samples of sulfides). The  $D_{Nd}/D_{Sm}$  ratio value equal to 1.65 is the mean value of the whole analyzed collection (80 samples), and the  $D_{Nd}/D_{Sm}$  ratio value equal to 1.15 is a value with no regard to redeposited and hydrothermal sulfides (a mean value taken from 66 samples). Thus, the mean value of the  $D_{Nd}/D_{Sm}$  ratio is 1.4, which perfectly matches the  $D_{Nd}/D_{Sm}$  ratio value calculated earlier only for the sulfides from the Cu-Ni-PGE complexes of the Fennoscandian Shield (45 samples). Furthermore, a  $D_{Nd}/D_{Sm}$  ratio value of 1.4 is an ideal match with an interval of values that were obtained earlier as the result of the experiment with sulfide liquids [94]. The paper presented the dependence of Nd and Sm distribution coefficients on FeO content and temperature. It was experimentally determined that the  $D_{Nd}/D_{Sm}$  ratio in sulfide liquid increases and approaches a 1.3–1.5 range of values [94] when the temperature decreases and the pressure is 1.5 GPa. This may cause the differences in Sm and Nd distribution coefficients for different sulfides during their sequential formation, depending on the temperature. Actually, we determined a trend of an increasing  $D_{Nd}/D_{Sm}$  ratio in a sequence of pyrite–chalcopyrite–pyrrhotine–pentlandite from 0.96 for pyrite to 1.93 for pentlandite [1] regarding the analyzed sulfide minerals.

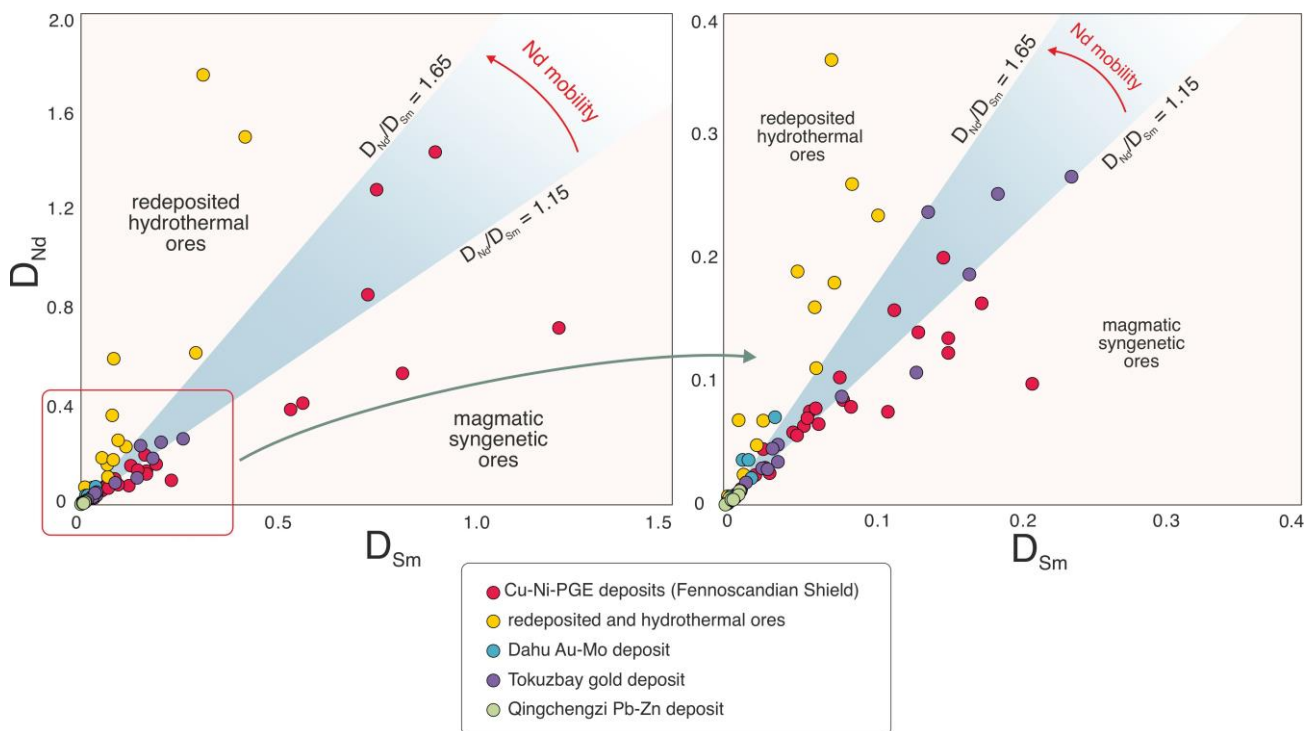


**Figure 3.** Partition coefficients  $D_{Nd}$ – $D_{Sm}$  in sulfide minerals from the Cu-Ni-PGE deposits of the Fennoscandian Shield and hydrothermal Qingchengzi Pb-Zn (northeastern China) deposit [18], Tokuzbay gold deposit [6] (south Altai, northwest China), and Dahu Au-Mo deposit [7].

This effect opens perspectives to reconstruct a possible sequence of sulfide crystallization and define the conditions for ore formation within intrusive complexes of various ages and geneses. For example, three stages of mineral formation are determined for the Kun-Manje Cu-Ni deposit (Russia) with a general sequence of pyrite–chalcopyrite–pyrrhotine–pentlandite [95]. The ore mineral formation sequence of pyrite–chalcopyrite–pyrrhotine is also determined for the Irankuh Zn-Pb deposit (Iran), Koudiat Aïcha Zn-Cu-Pb deposit (Mo-

rocco), and Shanggong Gold Deposit (China) [87,96,97]. Further increases in the  $D_{Nd}/D_{Sm}$  ratio above the values of 2.0–2.5 (with decreasing temperature) probably correspond to a hydrothermal process. The analysis of the obtained data showed that, generally, the  $D_{Nd}/D_{Sm}$  ratio value increases sharply in the case of minerals from recent processes that correspond to the redeposition of ores, metamorphism, or hydrothermal impact. This type of  $D_{Nd}/D_{Sm}$  behavior was demonstrated for the sulfides from the magmatic Cu-Ni deposits of Nyud (Monchegorsk ore district, Russia) and Ahmavaara (Finland). The  $D_{Nd}/D_{Sm}$  ratios have a mean value of 1.3 in sulfides from the syngenetic ores of the Ahmavaara deposit, whereas the  $D_{Nd}/D_{Sm}$  ratio value lies within the range of 2.2–7.7 for the redeposited ore (Figure 4). A similar pattern may be observed concerning the sulfides from the Nyud deposit. The  $D_{Nd}/D_{Sm}$  ratio has a value of 1.3 in sulfides from the syngenetic ores, whereas the metamorphosed ores indicate increasing  $D_{Nd}/D_{Sm}$  ratio values of 2.2–2.6 (Figure 4).

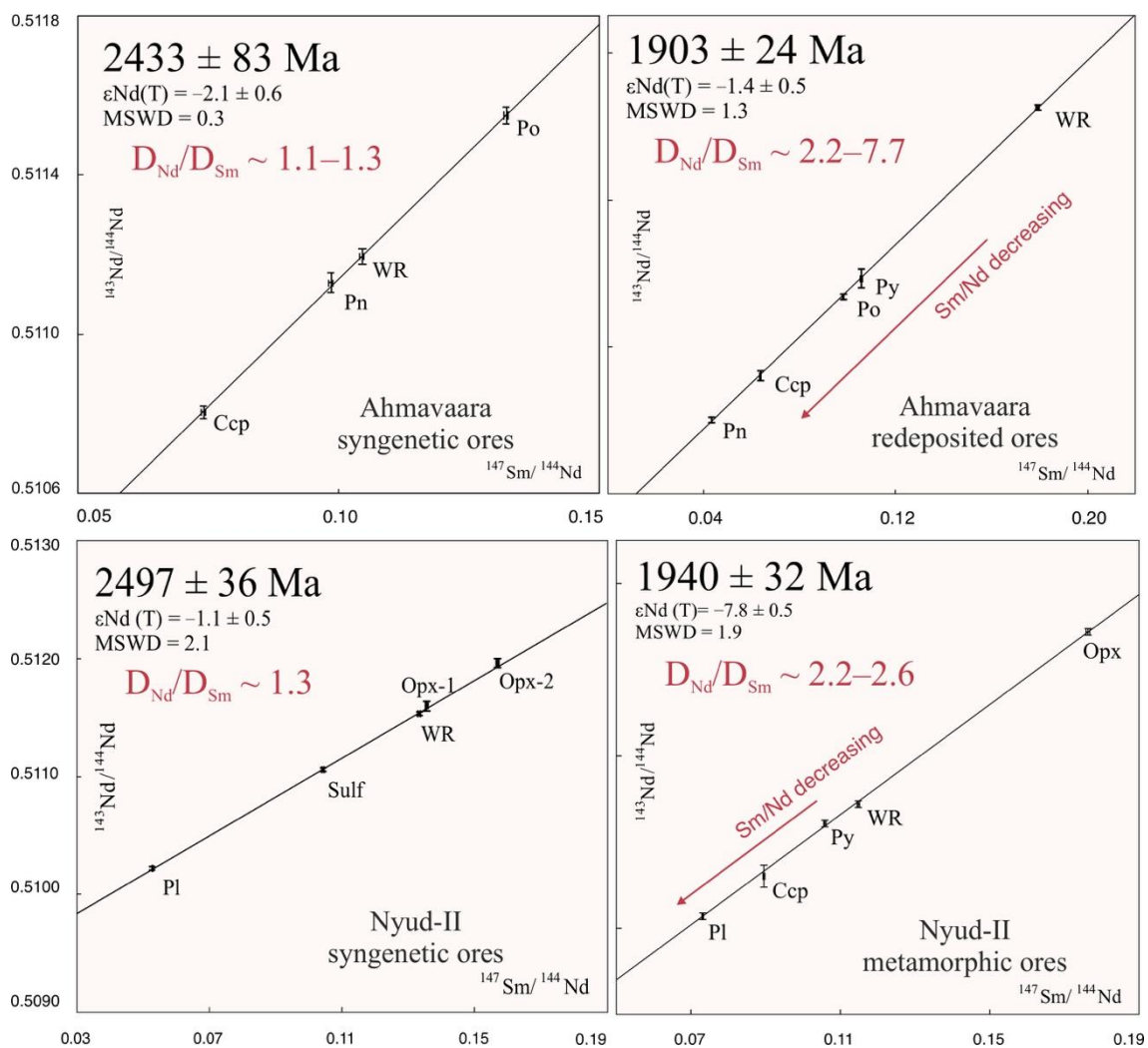


**Figure 4.** Mineral Sm-Nd isochrones for Ahmavaara and Nyud-II Cu-Ni deposits and  $D_{Nd}/D_{Sm}$  ratios for syngenetic and redeposited (or metamorphic) ores.

The same effect may be noticed at the Middle Devonian gold deposit of Tokuzbai (Southern Altai, China), where the  $D_{Nd}/D_{Sm}$  ratio increases as a result of the selective accumulation of Nd (in relation to Sm). Earlier, a complex Nd-Sr-Pb study was carried out concerning the sulfides and their host rocks from this deposit [6]. This study allows us to calculate the  $D_{Nd}/D_{Sm}$  coefficients and show that the revealed effect of selective Nd accumulation at the recent stages of sulfide mineral formation is of universal character. Furthermore, we have age values for the host rocks and the age of sulfide mineralization

occurrence (292 Ma [62], defined by the  $^{39}\text{Ar}/^{40}\text{Ar}$  method) for the studied deposit. Thus, we have the complete data necessary for the  $D_{\text{Nd}}/D_{\text{Sm}}$  coefficient calculation.

The calculation showed that the  $D_{\text{Nd}}/D_{\text{Sm}}$  ratios do not exceed the mean value of 1.3–1.5 regarding the primary disseminated mineralization in the hosting metasediments and diorite dikes. At the same time, the  $D_{\text{Nd}}/D_{\text{Sm}}$  ratio values increase to 2.3–8.5 for the late pyrites and chalcopyrites of the main ore stage from the diorite dikes. This indicates the concordance between the source of ore fluid and the diorite dike matter, which is one of the most important conclusions of the paper [6]. Neodymium and samarium behave the same way in some sulfide ores of the Kotselvaara deposit (Pechenga) and in the pyrites of the Dahu Au-Mo deposit (Table 1), as well. The observed selective Nd accumulation indicates a secondary hydrothermal or metamorphic impact, which led to the increased mobility and migration of Nd. Generally, chemical sulfide remobilization associated with the high mobility of certain elements was previously described for sphalerites [98].

This process causes the relative accumulation of Nd in comparison with Sm and a consequential increase in the  $D_{\text{Nd}}/D_{\text{Sm}}$  ratio. At the isotopic system level, this leads to a sufficient reduction in the Sm/Nd ratio for such secondary sulfides, their figurative points at isochrones aiming to an area of low  $^{147}\text{Sm}/^{144}\text{Nd}$  values (Figures 4 and 5).

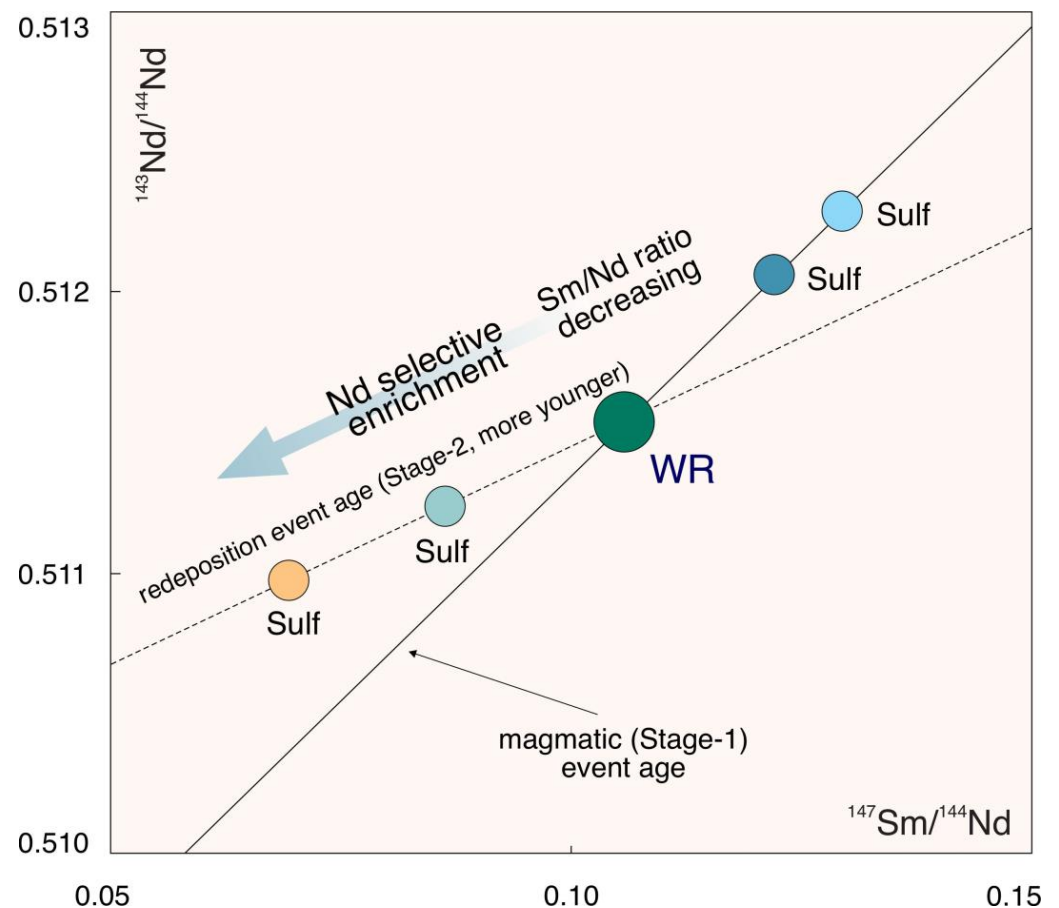


**Figure 5.** Chart demonstrating the effect of selective enrichment by neodymium in a hypothetical isochronous diagram. The process of relative Nd enrichment in comparison with Sm leads to a reduction in the Sm/Nd ratio for redeposited sulfides (Stage-2). In this case, the sulfide figurative points at an isochron often aim to the area of low  $^{147}\text{Sm}/^{144}\text{Nd}$  ratio values. In this respect, the syngenetic ores form an isochron that corresponds to the age of the formation of the ore at the magmatic stage (Stage-1).

#### 4.4. Nd and Sm in Magmatic Sulfides

Sulfides from the magmatic Cu-Ni-PGE complexes feature a more characteristic predominant (selective) accumulation of Nd in the sequence of pyrite–chalcopyrite–pyrrhotine–pentlandite, which corresponds to the most probable script of ore formation in intrusive complexes [1].

The crystallization of sulfides from the sulfide liquid happens at temperatures of 1200–1100 °C, where monosulfide solid solution (MSS) and Cu-rich residual melt form first, then the association recrystallizes into pyrrhotine, pentlandite, and chalcopyrite at temperatures below 650 °C [99]. Nd partially migrates from the Cu-rich melt to MSS during the separation of sulfide liquid into the Cu-rich melt and MSS (Figure 6). Then, the system keeps cooling down to a temperature below 650 °C, and there occurs the formation of chalcopyrite and the decomposition of MSS to pyrrhotine and pentlandite. In this case, pentlandite formation takes place at the late stages between pyrrhotine and chalcopyrite. Nd migrates to pentlandite from the neighboring minerals (chalcopyrite and pyrrhotine), thus causing the consequential increase in the  $D_{Nd}/D_{Sm}$  ratio from early sulfides (chalcopyrite, pyrrhotine) to late pentlandite (Figure 6). This scheme of the enrichment of late magmatic sulfides by Nd provides a reasonable explanation for the higher  $D_{Nd}/D_{Sm}$  ratios in pentlandite and pyrrhotine in relation to chalcopyrite and pyrite, which are often formed at the early stages of ore formation.

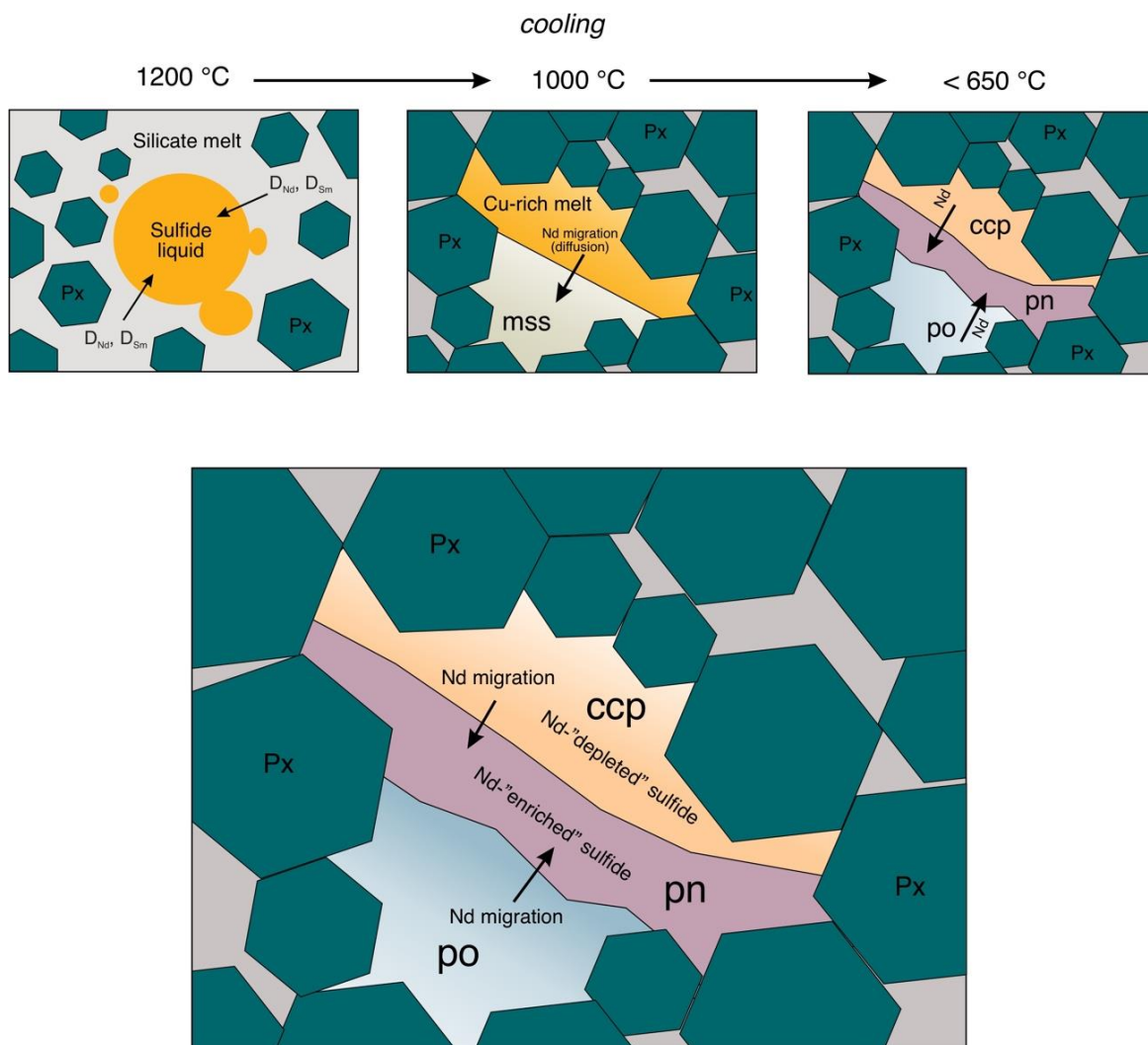


**Figure 6.** Chart of neodymium migration (diffusion) in magmatic sulfides in the course of sulfide-silicate liquid cooling. Px—pyroxene; ccp—chalcopyrite; pn—pentlandite; po—pyrrhotine.

#### 4.5. Nd and Sm in Hydrothermal Sulfides

Data on REE mobility in a system of magmatic–hydrothermal fluids [19] provide important conclusions that support our hypothesis of the selective accumulation of more mobile Nd in sulfides from the deposits closely associated with hydrothermal and metasomatic processes. Moreover, several ore-forming fluids, which form different generations of sulfides, are often revealed, and the REE composition may be subject to local physical and chemical conditions, i.e., temperature,  $fO_2$ , and pH [19,100,101].

Rather than high-temperature sulfides from mafic–ultramafic complexes, the hydrothermal sulfides are likely to feature a more characteristic REE accumulation in fluid inclusions and in crystal lattice defects besides the REE isomorphism. Taking into consideration a sufficient Nd interchange between the ore and host rocks [6] that may occur in the course of the hydrothermal process, the total effect of the Nd enrichment of sulfides will be more observable than that of the sulfides from the magmatic mafic–ultramafic complexes (Figure 7).

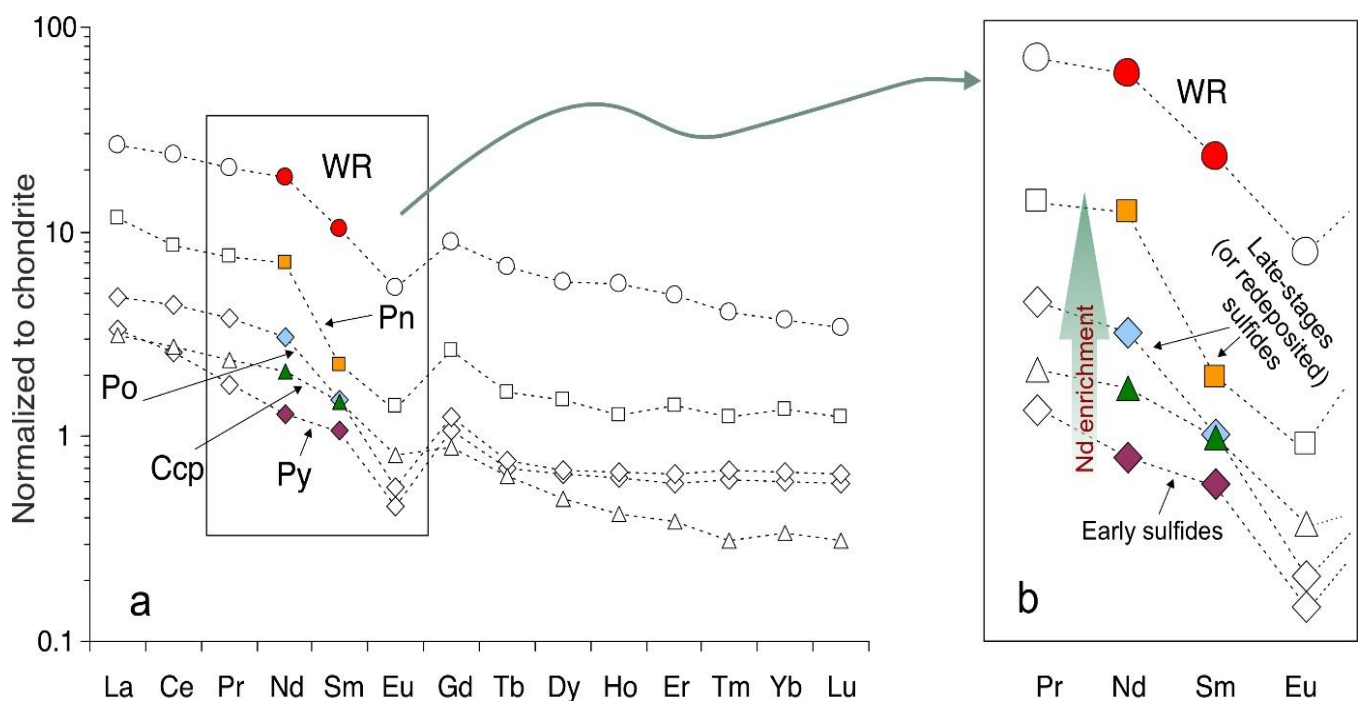


**Figure 7.** The effect of the Nd enrichment of sulfides from the magmatic mafic–ultramafic complexes (a) and that of the sulfides from different stages of the formation of minerals from the hydrothermal deposits (b). Sulfides from the magmatic Cu–Ni–PGE complexes feature a predominant (selective) accumulation of Nd in the sequence of pyrite–chalcopyrite–pyrrhotite–pentlandite, which corresponds to the most probable script of ore formation in intrusive complexes. The sulfides from hydrothermal deposits feature a more significant Nd enrichment effect that is closely associated with ore-forming fluids, which cause the formation of sulfide mineralization in several stages.

Thus, the higher mobility of light REE, fluid inclusions in sulfides, and active neodymium interchange between the host rocks and ores altogether may be treated as control factors of REE accumulation in sulfides with vividly expressed selective neodymium enrichment. This leads to considerable decreases in the Sm/Nd ratio (aiming at the 0.06–0.02 range of values) in similar sulfides, which is a “fingerprint” of a more recent process.

## 5. Conclusions

- (1) The  $D_{Nd}/D_{Sm}$  ratio is shown to increase for the sulfide minerals of late processes, which correspond to the redeposition of ores or hydrothermal or metamorphic impact. This process causes relative Nd enrichment in relation to Sm and the consequent increase in the  $D_{Nd}/D_{Sm}$  ratio for the sulfide minerals of late processes.
- (2) Sulfides from magmatic Cu-Ni-PGE complexes feature a more characteristic selective Nd accumulation in a sequence of pyrite–chalcopyrite–pyrrhotine–pentlandite, which corresponds to the most probable sequence of ore formation in magmatic complexes.
- (3) The hydrothermal sulfides feature a more characteristic REE accumulation in fluid and silicate inclusions and in crystal lattice defects. The total effect of the Nd enrichment of such sulfides will be more observable than that of the sulfides from the magmatic complexes.
- (4) The mineral/rock partition coefficients for Nd and Sm (the  $D_{Nd}/D_{Sm}$  ratio) in sulfides may serve as a prospective tool for the reconstruction of the sulfide mineral formation and geochemical substantiation of possible sources of ore-forming fluids for the deposits of various genetic types.

**Funding:** This research was funded by the Ministry of Science and Higher Education of the Russian Federation (project 0226-2019-0053).

**Acknowledgments:** The author expresses his appreciation to T.B. Bayanova, Head of the Laboratory of Geochronology and Isotope Geochemistry (Geological Institute of the Kola Science Centre, Russian Academy of Sciences), for general guidance on the studies and assistance during their implementation. The author thanks O.G. Sherstenikova and N.A. Ekimova (Geological Institute of the Kola Science Centre) for their help in the chemical preparation of the rocks and minerals; L.I. Koval (Geological Institute of the Kola Science Centre) for the extraction of the mineral fractions and grinding of the rocks. The author is also grateful to V.V. Chaschin, E.L. Kunakkuzin, E.N. Steshenko, E.S. Borisenko, and L.I. Nerovich for their help and advice during the field investigation, preliminary sample preparation, and analytical research. I am grateful to the Academic Editors and three anonymous reviewers for their help and comments, which improved the manuscript.

**Conflicts of Interest:** The author declares no conflict of interest.

## References

1. Serov, P.A.; Bayanova, T.B. The Sulfide/Silicate Coefficients of Nd and Sm: Geochemical “Fingerprints” for the Syn- and Epigenetic Cu-Ni-(PGE) Ores in the NE Fennoscandian Shield. *Minerals* **2021**, *11*, 1069. [[CrossRef](#)]
2. Ekimova, N.A.; Serov, P.A.; Bayanova, T.B.; Elizarova, I.R.; Mitrofanov, F.P. New Data on Distribution of REEs in Sulfide Minerals and Sm-Nd Dating of Ore Genesis of Layered Basic Intrusions. *Dokl. Earth Sci.* **2011**, *436*, 28–31. [[CrossRef](#)]
3. Steshenko, E.N.; Nikolaev, A.I.; Bayanova, T.B.; Drogobuzhskaya, S.V.; Chashchin, V.V.; Serov, P.A.; Lyalina, L.M.; Novikov, A.I. The Paleoproterozoic Kandalaksha Anorthosite Massif: New U–Pb (ID–TIMS) Data and Geochemical Features of Zircon. *Dokl. Earth Sci.* **2017**, *477*, 1454–1457. [[CrossRef](#)]
4. Bayanova, T.; Korchagin, A.; Mitrofanov, A.; Serov, P.; Ekimova, N.; Nitkina, E.; Kamensky, I.; Elizarov, D.; Huber, M. Long-Lived Mantle Plume and Polyphase Evolution of Palaeoproterozoic PGE Intrusions in the Fennoscandian Shield. *Minerals* **2019**, *9*, 59. [[CrossRef](#)]
5. Mitrofanov, F.P.; Bayanova, T.B.; Ludden, J.N.; Korchagin, A.U.; Chashchin, V.v.; Nerovich, L.I.; Serov, P.A.; Mitrofanov, A.F.; Zhironov, D.v. Origin and Exploration of the Kola PGE-bearing Province. In *Ore Deposits: Origin, Exploration, and Exploitation*; Decrée, S., Robb, L., Eds.; Wiley: New York, NY, USA, 2019; pp. 1–36.
6. Aibai, A.; Deng, X.; Pirajno, F.; Han, S.; Liu, W.; Li, X.; Chen, X.; Wu, Y.; Liu, J.; Chen, Y. Origin of Ore-Forming Fluids of Tokuzbay Gold Deposit in the South Altai, Northwest China: Constraints from Sr–Nd–Pb Isotopes. *Ore Geol. Rev.* **2021**, *134*, 104165. [[CrossRef](#)]
7. Ni, Z.Y.; Chen, Y.J.; Li, N.; Zhang, H. Pb–Sr–Nd Isotope Constraints on the Fluid Source of the Dahu Au–Mo Deposit in Qinling Orogen, Central China, and Implication for Triassic Tectonic Setting. *Ore Geol. Rev.* **2012**, *46*, 60–67. [[CrossRef](#)]
8. Yang, J.H.; Zhou, X.H. Rb–Sr, Sm–Nd, and Pb Isotopes Systematics of Pyrite: Implications for the Age and Genesis of Lode Gold Deposits. *Geology* **2002**, *29*, 711–714. [[CrossRef](#)]
9. Morgan, J.W.; Wandless, G.A. Rare Earth Element Distribution in Some Hydrothermal Minerals: Evidence for Crystallographic Control. *Geochim Cosmochim Acta* **1980**, *44*, 973–980. [[CrossRef](#)]
10. Kong, P.; Deloule, E.; Palme, H. REE-Bearing Sulfide in Bishunpur (LL3.1), a Highly Unequilibrated Ordinary Chondrite. *Earth Planet Sci. Lett.* **2000**, *177*, 1–7. [[CrossRef](#)]

11. Chen, G.; Shao, W.; Sun, D. *Genetic Mineralogy of Gold Deposits in Jiaodong Region with Emphasis on Gold Prospecting*; Chongqing Publishing House: Chongqing, China, 1989.
12. Rimskaya-Korsakova, M.N.; Dubinin, A.V. Rare Earth Elements in Sulfides of Submarine Hydrothermal Vents of the Atlantic Ocean. *Dokl. Earth Sci.* **2003**, *389*, 432–436.
13. Cao, Z.; Cao, H.; Tao, C.; Li, J.; Yu, Z.; Shu, L. Rare Earth Element Geochemistry of Hydrothermal Deposits from Southwest Indian Ridge. *Acta Oceanol. Sin.* **2012**, *31*, 62–69. [[CrossRef](#)]
14. Jiao, Q.; Wang, L.; Deng, T.; Xu, D.; Chen, G.; Yu, D.; Ye, T.; Gao, Y. Origin of the Ore-Forming Fluids and Metals of the Hetai Goldfield in Guangdong Province of South China: Constraints from C-H-O-S-Pb-He-Ar Isotopes. *Ore Geol. Rev.* **2017**, *88*, 674–689. [[CrossRef](#)]
15. Ruan, B.; Liao, M.; Sun, B.; Chen, C. Origin and Nature of Parental Magma and Sulfide Segregation of the Baixintan Magmatic Ni–Cu Sulfide Deposit, Southern Central Asian Orogenic Belt (Caob), Nw China: Insights from Mineral Chemistry of Chromite and Silicate Minerals. *Minerals* **2020**, *10*, 1050. [[CrossRef](#)]
16. Wang, S.; Li, H.; Zhai, S.; Yu, Z.; Cai, Z. Geochemical Features of Sulfides from the Deyin-1 Hydrothermal Field at the Southern Mid-Atlantic Ridge near 15°S. *J. Ocean Univ. China* **2017**, *16*, 1043–1054. [[CrossRef](#)]
17. Zeng, Z.; Ma, Y.; Yin, X.; Selby, D.; Kong, F.; Chen, S. Factors Affecting the Rare Earth Element Compositions in Massive Sulfides from Deep-Sea Hydrothermal Systems. *Geochim. Geophys. Geosystems.* **2015**, *18*, 1541–1576. [[CrossRef](#)]
18. Xu, L.; Yang, J.H.; Zeng, Q.D.; Xie, L.W.; Zhu, Y.S.; Li, R.; Li, B. Pyrite Rb-Sr, Sm-Nd and Fe Isotopic Constraints on the Age and Genesis of the Qingchengzi Pb-Zn Deposits, Northeastern China. *Ore Geol. Rev.* **2020**, *117*, 103324. [[CrossRef](#)]
19. Zhao, K.-D.; Jiang, S.-Y. Rare Earth Element and Yttrium Analyses of Sulfides from the Dachang Sn-Polymetallic Ore Field, Guangxi Province, China: Implication for Ore Genesis. *Geochim. J.* **2007**, *41*, 121–134. [[CrossRef](#)]
20. Liu, K.; Yang, R.; Chen, W.; Liu, R.; Tao, P. Trace Element and REE Geochemistry of Sanshenjiang Gold Deposit, Southeastern Guizhou Province, China. *Chin. J. Geochem.* **2014**, *33*, 109–118. [[CrossRef](#)]
21. Karykowski, B.T.; Maier, W.D.; Groshev, N.Y.; Barnes, S.-J.; Pripachkin, P.v.; McDonald, I.; Savard, D. Critical Controls on the Formation of Contact-Style PGE-Ni-Cu Mineralization: Evidence from the Paleoproterozoic Monchegorsk Complex, Kola Region, Russia. *Econ. Geol.* **2018**, *113*, 911–935. [[CrossRef](#)]
22. Nerovich, L.I.; Bayanova, T.B.; Serov, P.A.; Elizarov, D.v. Magmatic Sources of Dikes and Veins in the Moncha Tundra Massif, Baltic Shield: Isotopic-Geochronologic and Geochemical Evidence. *Geochim. Int.* **2014**, *52*, 548–566. [[CrossRef](#)]
23. Sharkov, E.v.; Chistyakov, A.v. Geological and Petrological Aspects of Ni-Cu-PGE Mineralization in the Early Paleoproterozoic Monchegorsk Layered Mafic-Ultramafic Complex, Kola Peninsula. *Geol. Ore Depos.* **2014**, *56*, 147–168. [[CrossRef](#)]
24. Yang, S.-H.; Hanski, E.; Li, C.; Maier, W.D.; Huhma, H.; Mokrushin, A.v.; Latypov, R.; Lahaye, Y.; O'Brien, H.; Qu, W.-J. Mantle Source of the 2.44–2.50-Ga Mantle Plume-Related Magmatism in the Fennoscandian Shield: Evidence from Os, Nd, and Sr Isotope Compositions of the Monchepluton and Kemi Intrusions. *Min. Depos.* **2016**, *51*, 1055–1073. [[CrossRef](#)]
25. Hanski, E.; Huhma, H.; Smolkin, V.F.; Vaasjoki, M. The Age of the Ferropicritic Volcanics and Comagmatic Ni-Bearing Intrusions at Pechenga, Kola Peninsula, U.S.S.R. *Bull. Geol. Soc. Finl.* **1990**, *62*, 123–133. [[CrossRef](#)]
26. Walker, R.J.; Morgan, J.W.; Hanski, E.J.; Smolkin, V.F. Re-Os Systematics of Early Proterozoic Ferropicrites, Pechenga Complex, Northwestern Russia: Evidence for Ancient 187Os-Enriched Plumes. *Geochim. Cosmochim. Acta* **1997**, *61*, 3145–3160. [[CrossRef](#)]
27. Sharkov, E.v.; Smolkin, V.F. The Early Proterozoic Pechenga-Varzuga Belt: A Case of Precambrian Back-Arc Spreading. *Precambrian Res.* **1997**, *82*, 133–151. [[CrossRef](#)]
28. Smolkin, V.F.; Lokhov, K.I.; Skublov, S.G.; Sergeeva, L.Y.; Lokhov, D.K.; Sergeev, S.A. Paleoproterozoic Keulik–Kenirim Ore-Bearing Gabbro–Peridotite Complex, Kola Region: A New Occurrence of Ferropicritic Magmatism. *Geol. Ore Depos.* **2018**, *60*, 142–171. [[CrossRef](#)]
29. Neradovsky, Y.; Alekseeva, S.; Chernousenko, E. Mineralogy and Process Properties of Kolvitsky Titanomagnetite Ore. *IOP Conf. Ser. Earth Environ. Sci.* **2019**, *262*, 012050. [[CrossRef](#)]
30. Voitekhovskiy, Y.L.; Neradovskiy, Y.N.; Grishin, N.N.; Rakitina, E.Y.; Kasikov, A.G. Kolvitsa Field (Geology, Material Composition of Ores). *Vestn. MSTU* **2014**, *17*, 271–278.
31. Schissel, D.; Tsvetkov, A.A.; Mitrofanov, F.P.; Korchagin, A.U. Basal Platinum-Group Element Mineralization in the Federov Pansky Layered Mafic Intrusion, Kola Peninsula, Russia. *Econ. Geol.* **2002**, *97*, 1657–1677. [[CrossRef](#)]
32. Groshev, N.; Karykowski, B. The Main Anorthosite Layer of the West-Pana Intrusion, Kola Region: Geology and U-Pb Age Dating. *Minerals* **2019**, *9*, 71. [[CrossRef](#)]
33. Serov, P.A. Paleoproterozoic Pt-Pd Fedorovo-Pansky and Cu-Ni-Cr Monchegorsk Ore Complexes: Age, Metamorphism, and Crustal Contamination According to Sm-Nd Data. *Minerals* **2021**, *11*, 1410. [[CrossRef](#)]
34. Amelin, Y.V.; Heaman, L.M.; Semenov, V.S. U-Pb Geochronology of Layered Mafic Intrusions in the Eastern Baltic Shield: Implications for the Timing and Duration of Paleoproterozoic Continental Rifting. *Precambrian Res.* **1995**, *75*, 31–46. [[CrossRef](#)]
35. Huhma, H.; Cliff, R.A.; Perttunen, V.; Sakko, M. Sm-Nd and Pb Isotopic Study of Mafic Rocks Associated with Early Proterozoic Continental Rifting: The Peräpohja Schist Belt in Northern Finland. *Contrib. Mineral. Petrol.* **1990**, *104*, 369–379. [[CrossRef](#)]
36. Halkoaho, T.A.A.; Alapieti, T.T.; Lahtinen, J.J. The Sompujärvi PGE Reef in the Penikat Layered Intrusion, Northern Finland. *Miner. Pet.* **1990**, *42*, 39–55. [[CrossRef](#)]
37. Iljina, M.; Maier, W.D.; Karinen, T. PGE-(Cu-Ni) Deposits of the Tornio-Näränkäväära Belt of Intrusions (Portimo, Penikat, and Koillismaa). In *Mineral Deposits of Finland*; Elsevier: Amsterdam, Netherlands, 2015; pp. 133–164. ISBN 9780124104761.

38. Hanski, E.; Walker, R.J.; Huhma, H.; Suominen, I. The Os and Nd Isotopic Systematics of c. 2.44 Ga Akanvaara and Koitelainen Mafic Layered Intrusions in Northern Finland. *Precambrian Res.* **2001**, *109*, 73–102. [[CrossRef](#)]
39. Balashov, Y.A.; Bayanova, T.B.; Mitrofanov, F.P. Isotope Data on the Age and Genesis of Layered Basic-Ultrabasic Intrusions in the Kola Peninsula and Northern Karelia, Northeastern Baltic Shield. *Precambrian Res.* **1993**, *64*, 197–205. [[CrossRef](#)]
40. Bayanova, T.B. Baddeleyite: A Promising Geochronometer for Alkaline and Basic Magmatism. *Petrology* **2006**, *14*, 187–200. [[CrossRef](#)]
41. Bekker, A.; Grokhovskaya, T.L.; Hiebert, R.; Sharkov, E.v.; Bui, T.H.; Stadnek, K.R.; Chashchin, V.v.; Wing, B.A. Multiple Sulfur Isotope and Mineralogical Constraints on the Genesis of Ni-Cu-PGE Magmatic Sulfide Mineralization of the Monchegorsk Igneous Complex, Kola Peninsula, Russia. *Min. Depos.* **2016**, *51*, 1035–1053. [[CrossRef](#)]
42. Chashchin, V.v.; Bayanova, T.B.; Mitrofanov, F.P.; Serov, P.A. Low-Sulfide PGE Ores in Paleoproterozoic Monchegorsk Pluton and Massifs of Its Southern Framing, Kola Peninsula, Russia: Geological Characteristic and Isotopic Geochronological Evidence of Polychronous Ore–Magmatic Systems. *Geol. Ore Depos.* **2016**, *58*, 37–57. [[CrossRef](#)]
43. Hanski, E.; Huhma, H.; Vaasjoki, M. Geochronology of Northern Finland: A Summary and Discussion. *Spec. Pap. Geol. Surv. Finl.* **2001**, *33*, 255–279.
44. Hanski, E.J. Evolution of the Palaeoproterozoic (2.50–1.95 Ga) Non-Orogenic Magmatism in the Eastern Part of the Fennoscandian Shield. In *Reading the Archive of Earth's Oxygenation*; Melezhik, V.A., Prave, A.R., Fallick, A.E., Kump, L.R., Strauss, H., Lepland, A., Hanski, E.J., Eds.; Springer: Berlin/Heidelberg, Germany, 2013; pp. 179–245. ISBN 978-3-642-29682-6.
45. Smith, W.D.; Maier, W.D. The Geotectonic Setting, Age and Mineral Deposit Inventory of Global Layered Intrusions. *Earth Sci. Rev.* **2021**, *220*, 103736. [[CrossRef](#)]
46. Lauri, L.S.; Mikkola, P.; Karinen, T. Early Paleoproterozoic Felsic and Mafic Magmatism in the Karelian Province of the Fennoscandian Shield. *Lithos* **2012**, *151*, 74–82. [[CrossRef](#)]
47. Moilanen, M.; Hanski, E.; Konnunaho, J.; Yang, S.H.; Törmänen, T.; Li, C.; Zhou, L.M. Re-Os Isotope Geochemistry of Komatiite-Hosted Ni-Cu-PGE Deposits in Finland. *Ore Geol. Rev.* **2019**, *105*, 102–122. [[CrossRef](#)]
48. Moilanen, M.; Hanski, E.; Konnunaho, J.; Törmänen, T.; Yang, S.-H.; Lahaye, Y.; O'Brien, H.; Illikainen, J. Composition of Iron Oxides in Archean and Paleoproterozoic Mafic-Ultramafic Hosted Ni-Cu-PGE Deposits in Northern Fennoscandia: Application to Mineral Exploration. *Min. Depos.* **2020**, *55*, 1515–1534. [[CrossRef](#)]
49. Peltonen, P.; Brüggmann, G. Origin of Layered Continental Mantle (Karelian Craton, Finland): Geochemical and Re–Os Isotope Constraints. *Lithos* **2006**, *89*, 405–423. [[CrossRef](#)]
50. Puchtel, I.; Brüggmann, G.; Hofmann, A.; Kulikov, V.; Kulikova, V. Os Isotope Systematics of Komatiitic Basalts from the Vetreny Belt, Baltic Shield: Evidence for a Chondritic Source of the 2.45 Ga Plume. *Contrib. Miner. Petrol.* **2001**, *140*, 588–599. [[CrossRef](#)]
51. Vogel, D.C.; Vuollo, J.I.; Alapieti, T.T.; James, R.S. Tectonic, Stratigraphic, and Geochemical Comparisons between ca. 2500–2440Ma Mafic Igneous Events in the Canadian and Fennoscandian Shields. *Precambrian Res.* **1998**, *92*, 89–116. [[CrossRef](#)]
52. Lahtinen, R.; Garde, A.A.; Victor, M. Paleoproterozoic Evolution of Fennoscandia and Greenland. *Episodes* **2008**, *31*, 20–28. [[CrossRef](#)]
53. Melezhik, V.A.; Prave, A.R.; Fallick, A.E.; Hanski, E.J.; Lepland, A.; Kump, L.R.; Strauss, H. *Reading the Archive of Earth's Oxygenation*; Frontiers in Earth Sciences; Melezhik, V., Prave, A.R., Hanski, E.J., Fallick, A.E., Lepland, A., Kump, L.R., Strauss, H., Eds.; Springer: Berlin/Heidelberg, Germany, 2013; Volume 7, ISBN 978-3-642-29658-1.
54. Abzalov, M.Z.; Both, R.A. The Pechenga Ni-Cu Deposits, Russia: Data on PGE and Au Distribution and Sulphur Isotope Compositions. *Miner. Pet.* **1997**, *61*, 119–143. [[CrossRef](#)]
55. Balabonin, N.L.; Distler, V.V.; Dokuchaeva, V.S.; Neradovsky, Y.N.; Orsoev, D.A.; Osokin, A.S.; Filimonova, A.A.; Yakovlev, Y.N.; Yakovleva, A.K. *Mineralogy of Sulfide Copper-Nickel Deposits of the Kola Peninsula*; Gorbunov, G.I., Ed.; Nauka: Leningrad, Russia, 1981.
56. Hickey, R.L.; Frey, F.A. Geochemical Characteristics of Boninite Series Volcanics: Implications for Their Source. *Geochim. Cosmochim. Acta* **1982**, *46*, 2099–2115. [[CrossRef](#)]
57. Smolkin, V.F.; Mitrofanov, F.P. *Layered Intrusions of the Monchegorsk Ore District: Petrology, Mineralization, and Deep Structure*; Mitrofanov, F.P., Smolkin, V.F., Eds.; Kola Science Center RAS: Apatity, Russia, 2004.
58. Bayanova, T.B.; Nerovich, L.I.; Mitrofanov, F.P.; Zhavkov, V.A.; Serov, P.A. The Monchetundra Basic Massif of the Kola Region: New Geological and Isotope Geochronological Data. *Dokl. Earth Sci.* **2010**, *431*, 288. [[CrossRef](#)]
59. Li, Y.; Zhou, G.; Chai, F.M. LA-ICP-MS U-Pb Ages and Geological Implications of the Habahe Pluton at the Southern Margin of the Altay, Xinjiang. *Xinjiang Geology* **2010**, *30*, 146–151.
60. Zhou, N.-W.; Guo, X.-C.; He, G.-L. LA-ICP-MS Zircon U-Pb Ages of Two Types of Ore-Bearing Dykes in the Tuokuzibayi Gold Ore District in Habahe Area of Xinjiang and Their Geological Significance. *Geol. Bull. China* **2012**, *31*, 707–715.
61. Cai, K.; Sun, M.; Yuan, C.; Zhao, G.; Xiao, W.; Long, X.; Wu, F. Geochronological and Geochemical Study of Mafic Dykes from the Northwest Chinese Altai: Implications for Petrogenesis and Tectonic Evolution. *Gondwana Res.* **2010**, *18*, 638–652. [[CrossRef](#)]
62. Yan, S.; Chen, W.; Wang, Y.; Zhang, Z.; Chen, B. <sup>40</sup>Ar/<sup>39</sup>Ar dating and its significance of the Ertix gold metallogenic belt in the Altay Oregon, Xinjiang. *Acta Geol. Sin.* **2004**, *78*, 500–506.
63. Zhang, H.-F.; Ying, J.-F.; Tang, Y.-J.; Li, X.-H.; Feng, C.; Santosh, M. Phanerozoic Reactivation of the Archean North China Craton through Episodic Magmatism: Evidence from Zircon U–Pb Geochronology and Hf Isotopes from the Liaodong Peninsula. *Gondwana Res.* **2011**, *19*, 446–459. [[CrossRef](#)]

64. Zhai, M.; Santosh, M. Metallogeny of the North China Craton: Link with Secular Changes in the Evolving Earth. *Gondwana Res.* **2013**, *24*, 275–297. [[CrossRef](#)]
65. Fang, R.H. On the Ordered Liaohe Group Sequences. *Liaoning Geol.* **1993**, *2*, 97–119.
66. Duan, X.; Zeng, Q.; Yang, J.; Liu, J.; Wang, Y.; Zhou, L. Geochronology, Geochemistry and Hf Isotope of Late Triassic Magmatic Rocks of Qingchengzi District in Liaodong Peninsula, Northeast China. *J. Asian Earth Sci.* **2014**, *91*, 107–124. [[CrossRef](#)]
67. Fang, R.; He, S.; Fu, D. Nonferrous Metallic Ore Deposit in the East Liaoningsouth Jilin Early Proterozoic Rift. In *Geology of Coloured Metallic Mineral Deposits in North Margin of North China Terrain and Neighbor Area*; Rui, Z.Y., Shi, L.D., Fang, R.H., Eds.; Geological Publishing House: Beijing, China, 1994; pp. 54–64.
68. Zhao, H.-X.; Jiang, S.-Y.; Frimmel, H.E.; Dai, B.-Z.; Ma, L. Geochemistry, Geochronology and Sr–Nd–Hf Isotopes of Two Mesozoic Granitoids in the Xiaoqinling Gold District: Implication for Large-Scale Lithospheric Thinning in the North China Craton. *Chem. Geol.* **2012**, *294*, 173–189. [[CrossRef](#)]
69. Li, N.; Chen, Y.-J.; Fletcher, I.R.; Zeng, Q.-T. Triassic Mineralization with Cretaceous Overprint in the Dahu Au–Mo Deposit, Xiaoqinling Gold Province: Constraints from SHRIMP Monazite U–Th–Pb Geochronology. *Gondwana Res.* **2011**, *20*, 543–552. [[CrossRef](#)]
70. Kalinin, A.A.; Kaulina, T.v.; Serov, P.A. Comparison of Isotope Data Obtained with Sm–Nd and Re–Os Methods for Minerals and Rocks from the Ozernoe Ore Occurrence, Salla-Kuolajarvi Belt. *Vestn. MGTU* **2021**, *24*, 5–13. [[CrossRef](#)]
71. Raczek, I.; Jochum, K.P.; Hofmann, A.W. Neodymium and Strontium Isotope Data for USGS Reference Materials BCR-1, BCR-2, BHVO-1, BHVO-2, AGV-1, AGV-2, GSP-1, GSP-2 and Eight MPI-DING Reference Glasses. *Geostand. Geoanal. Res.* **2003**, *27*, 173–179. [[CrossRef](#)]
72. Tanaka, T.; Togashi, S.; Kamioka, H.; Amakawa, H.; Kagami, H.; Hamamoto, T.; Yuhara, M.; Orihashi, Y.; Yoneda, S.; Shimizu, H.; et al. JNdi-1: A Neodymium Isotopic Reference in Consistency with LaJolla Neodymium. *Chem. Geol.* **2000**, *168*, 279–281. [[CrossRef](#)]
73. Ludwig, K.R. Isoplot 3.75. A Geochronological Toolkit for Microsoft Excel. *Berkeley Geochronol. Cent. Spec. Publ.* **2012**, *4*, 71.
74. Bouvier, A.; Vervoort, J.D.; Patchett, P.J. The Lu–Hf and Sm–Nd Isotopic Composition of CHUR: Constraints from Unequilibrated Chondrites and Implications for the Bulk Composition of Terrestrial Planets. *Earth Planet Sci. Lett.* **2008**, *273*, 48–57. [[CrossRef](#)]
75. Goldstein, S.J.; Jacobsen, S.B. Nd and Sr Isotopic Systematics of River Water Suspended Material: Implications for Crustal Evolution. *Earth Planet Sci. Lett.* **1988**, *87*, 249–265. [[CrossRef](#)]
76. Elizarova, I.R.; Bayanova, T.B. Mass-Spectrometric REE Analysis in Sulphide Minerals. *J. Biol. Earth Sci.* **2012**, *2*, 45–49. [[CrossRef](#)]
77. Steshenko, E.N.; Bayanova, T.B.; Serov, P.A. The Paleoproterozoic Kandalaksha-Kolvitsa Gabbro-Anorthosite Complex (Fennoscandian Shield): New U–Pb, Sm–Nd, and Nd–Sr (ID-TIMS) Isotope Data on the Age of Formation, Metamorphism, and Geochemical Features of Zircon (LA-ICP-MS). *Minerals* **2020**, *10*, 254. [[CrossRef](#)]
78. Kunakkuzin, E.; Borisenko, E.; Nerovich, L.; Serov, P.; Bayanova, T.; Elizarov, D. The Origin and Evolution of Ore-Bearing Rocks in the Loppishnun Deposit (Monchetundra Massif, NE Fennoscandian Shield): Isotope Nd–Sr and REE Geochemical Data. *Minerals* **2020**, *10*, 286. [[CrossRef](#)]
79. Shannon, R.D. Revised Effective Ionic Radii and Systematic Studies of Interatomic Distances in Halides and Chalcogenides. *Acta Crystallogr. Sect. A* **1976**, *32*, 751–767. [[CrossRef](#)]
80. Jordens, A.; Cheng, Y.P.; Waters, K.E. A Review of the Beneficiation of Rare Earth Element Bearing Minerals. *Min. Eng.* **2013**, *41*, 97–114. [[CrossRef](#)]
81. She, H.; Fan, H.; Yang, K.; Liu, X.; Li, X.; Dai, Z.-H. Carbonatitic Footprints in the Bayan Obo REEs Deposit as Seen from Pyrite Geochemistry. *Precambrian Res.* **2022**, *379*, 106801. [[CrossRef](#)]
82. Borst, A.M.; Smith, M.P.; Finch, A.A.; Estrade, G.; Villanova-de-Benavent, C.; Nason, P.; Marquis, E.; Horsburgh, N.J.; Goodenough, K.M.; Xu, C.; et al. Adsorption of Rare Earth Elements in Regolith-Hosted Clay Deposits. *Nat. Commun.* **2020**, *11*, 4386. [[CrossRef](#)] [[PubMed](#)]
83. MacDonald, J.M.; Wheeler, J.; Harley, S.L.; Mariani, E.; Goodenough, K.M.; Crowley, Q.; Tatham, D. Lattice Distortion in a Zircon Population and Its Effects on Trace Element Mobility and U–Th–Pb Isotope Systematics: Examples from the Lewisian Gneiss Complex, Northwest Scotland. *Contrib. Miner. Petrol.* **2013**, *166*, 21–41. [[CrossRef](#)]
84. Mao, G.; Hua, R.; Gao, J.; Li, W.; Zhao, K.; Long, G.; Lu, H. Existing Forms of REE in Gold-Bearing Pyrite of the Jinshan Gold Deposit, Jiangxi Province, China. *J. Rare Earths* **2009**, *27*, 1079–1087. [[CrossRef](#)]
85. Silyanov, S.A.; Sazonov, A.M.; Tishin, P.A.; Lobastov, B.M.; Nekrasova, N.A.; Zvyagina, E.A.; Ryabukha, M.A. Trace Elements in Sulfides and Gold of the Olimpiada Deposit (Yenisei Ridge): Ore Substance Sources and Fluid Parameters. *Russ. Geol. Geophys.* **2021**, *62*, 306–323. [[CrossRef](#)]
86. Bai, Z.J.; Zhong, H.; Hu, R.Z.; Zhu, W.G. Early Sulfide Saturation in Arc Volcanic Rocks of Southeast China: Implications for the Formation of Co-Magmatic Porphyry–Epithermal Cu–Au Deposits. *Geochim. Cosmochim. Acta* **2020**, *280*, 66–84. [[CrossRef](#)]
87. Chen, Y.-J.; Pirajno, F.; Qi, J.-P. The Shangong Gold Deposit, Eastern Qinling Orogen, China: Isotope Geochemistry and Implications for Ore Genesis. *J. Asian Earth Sci.* **2008**, *33*, 252–266. [[CrossRef](#)]
88. Pirajno, F. *Hydrothermal Processes and Mineral Systems*; Springer: Dordrecht, The Netherlands, 2009; ISBN 978-1-4020-8612-0.
89. Serov, P.A.; Kadyrov, R.I.; Kalashnikov, A.O. Microtomography of Sulfide Minerals: Study of Internal Micro-Inclusions and the Consequences for Sm–Nd Dating of Ore-Genesis. In *Ultramafic-Mafic Complexes: Geology, Structure, Ore Potential*; Mokrushin, A.V., Ed.; Publishing House of the FRC KSC RAS: Apatity, Russia, 2022; pp. 91–93.

90. Verberne, R.; Reddy, S.M.; Saxey, D.W.; Fougereuse, D.; Rickard, W.D.A.; Quadir, Z.; Evans, N.J.; Clark, C. Dislocations in Minerals: Fast-Diffusion Pathways or Trace-Element Traps? *Earth Planet Sci. Lett.* **2022**, *584*, 117517. [[CrossRef](#)]
91. Serov, P.A.; Ekimova, N.A.; Bayanova, T.B.; Mitrofanov, F.P. Sulphide Minerals as New Sm-Nd Geochronometers for Ore Genesis Dating of Mafic-Ultramafic Layered Intrusions of Baltic Shield. *LITHOSPHERE* **2014**, *4*, 11–21.
92. Mills, R.A.; Elderfield, H. Rare Earth Element Geochemistry of Hydrothermal Deposits from the Active TAG Mound, 26°N Mid-Atlantic Ridge. *Geochim. Cosmochim. Acta* **1995**, *59*, 3511–3524. [[CrossRef](#)]
93. Marques, A.F.A.; Barriga, F.; Chavagnac, V.; Fouquet, Y. Mineralogy, Geochemistry, and Nd Isotope Composition of the Rainbow Hydrothermal Field, Mid-Atlantic Ridge. *Min. Depos.* **2006**, *41*, 52–67. [[CrossRef](#)]
94. Wohlers, A.; Wood, B.J. Uranium, Thorium and REE Partitioning into Sulfide Liquids: Implications for Reduced S-Rich Bodies. *Geochim. Cosmochim. Acta* **2017**, *205*, 226–244. [[CrossRef](#)]
95. Kotelnikov, A.E.; Kolmakova, D.A.; Kotelnikova, E.M. Determination of the Copper-Nickel Ores Formation Sequence of the Kun-Manye Deposit (Amur Region). *RUDN J. Eng. Res.* **2020**, *21*, 48–57. [[CrossRef](#)]
96. Essarraj, S.; Zoheir, B.; Steele-macinnis, M.; Frische, M.; Khalifa, A.; Ouadjou, A. Polymetallic Sulfide—Quartz Vein System in the Koudiat Aïcha Massive Sulfide Deposit, Jebilet Massif, Morocco: Microanalytical and Fluid Inclusion Approaches. *Minerals* **2022**, *12*, 1396. [[CrossRef](#)]
97. Liu, Y.C.; Song, Y.C.; Fard, M.; Zhou, L.M.; Hou, Z.Q.; Kendrick, M.A. Pyrite Re-Os Age Constraints on the Irankuh Zn-Pb Deposit, Iran, and Regional Implications. *Ore Geol. Rev.* **2019**, *104*, 148–159. [[CrossRef](#)]
98. Cave, B.; Lilly, R.; Hong, W. The Effect of Co-Crystallising Sulphides and Precipitation Mechanisms on Sphalerite Geochemistry: A Case Study from the Hilton Zn-Pb (Ag) Deposit, Australia. *Minerals* **2020**, *10*, 797. [[CrossRef](#)]
99. Holwell, D.A.; Fiorentini, M.L.; Knott, T.R.; McDonald, I.; Blanks, D.E.; Campbell McCuaig, T.; Gorczyk, W. Mobilisation of Deep Crustal Sulfide Melts as a First Order Control on Upper Lithospheric Metallogeny. *Nat. Commun.* **2022**, *13*, 573. [[CrossRef](#)]
100. Shelton, K.L.; Cavender, B.D.; Perry, L.E.; Schiffbauer, J.D.; Appold, M.S.; Burstein, I.; Fike, D.A. Stable Isotope and Fluid Inclusion Studies of Early Zn-Cu-(Ni-Co)-Rich Ores, Lower Ore Zone of Brushy Creek Mine, Viburnum Trend MVT District, Missouri, U.S.A.: Products of Multiple Sulfur Sources and Metal-Specific Fluids. *Ore Geol. Rev.* **2020**, *118*, 103358. [[CrossRef](#)]
101. Stoltnow, M.; Lüders, V.; de Graaf, S.; Niedermann, S. A Geochemical Study of the Sweet Home Mine, Colorado Mineral Belt, USA: Formation of Deep Hydrothermal Vein-Type Molybdenum Greisen and Base Metal Mineralization. *Min. Depos.* **2022**, *57*, 801–825. [[CrossRef](#)]